Geochemistry Geophysics Geosystems G3

Article
Volume 12, Number 12
30 December 2011
Q0AM02, doi:10.1029/2011GC003804
ISSN: 1525-2027

Published by AGU and the Geochemical Society

New ^{40}Ar/^{39}Ar age progression for the Louisville hot spot trail and implications for inter–hot spot motion

Anthony A. P. Koppers

College of Earth, Ocean and Atmospheric Sciences, Oregon State University, 104 Ocean Administration Building, Corvallis, Oregon 97331–5503, USA (akoppers@coas.oregonstate.edu)

Scripps Institution of Oceanography, University of California, San Diego, La Jolla, California 92093, USA

Molly D. Gowen and Lauren E. Colwell

College of Earth, Ocean and Atmospheric Sciences, Oregon State University, 104 Ocean Administration Building, Corvallis, Oregon 97331–5503, USA

Jeffrey S. Gee and Peter F. Lonsdale

Scripps Institution of Oceanography, University of California, San Diego, La Jolla, California 92093, USA

John J. Mahoney

School of Ocean and Earth Science and Technology, University of Hawai'i at Mānoa, Honolulu, Hawaii 96822, USA

Robert A. Duncan

College of Earth, Ocean and Atmospheric Sciences, Oregon State University, 104 Ocean Administration Building, Corvallis, Oregon 97331–5503, USA

[1] In this study we present 42 new ^{40}Ar/^{39}Ar incremental heating age determinations that contribute to an updated age progression for the Louisville seamount trail. Louisville is the South Pacific counterpart to the Hawaiian-Emperor seamount trail, both trails representing intraplate volcanism over the same time interval (~80 Ma to present) and being examples of *primary* hot spot lineaments. Our data provide evidence for an age-progressive trend from 71 to 21 Ma. Assuming fixed hot spots, this makes possible a direct comparison to the Hawaiian-Emperor age progression and the most recent absolute plate motion (APM) model (WK08G) of *Wessel and Kroenke* (2008). We observe that for the Louisville seamount trail the measured ages are systematically older relative to both the WK08G model predictions and Hawaiian seamount ages, with offsets ranging up to 6 Myr. Taking into account the uncertainty about the duration of eruption and magmatic succession at individual Louisville volcanoes, these age offsets should be considered minimum estimates, as our sampling probably tended to recover the youngest lava flows. These large deviations point to either a contribution of inter–hot spot motion between the Louisville and Hawaiian hot spots or to a more easterly location of the Louisville hot spot than the one inferred in the WK08G model. Both scenarios are investigated in this paper, whereby the more eastern hot spot location (52.0°S, 134.5°W versus 52.4°S, 137.2°W) reduces the average age offset, but still results in a relatively large maximum offset of 3.7 Myr. When comparing the new ages to the APM models (S04P, S04G) by *Steinberger et al.* (2004) that attempt to compensate for the motion of hot spots in the Pacific (Hawaii) or globally (Hawaii, Louisville, Reunion and Walvis), the measured and predicted ages are more in agreement, showing only a maximum offset of 2.3 Myr with respect to the S04G model. At face value these more advanced APM models, which consider both plate and hot spot motions, therefore provide a better fit to the new Louisville age data. The fit is particularly good for seamounts younger than 50 Ma, a period for which there is little predicted motion for the Louisville hot spot and little inter–hot spot motion with Hawaii. However, discrepancies in the

Louisville age-distance record prior to 50 Ma indicate there is an extra source of inter–hot spot motion between Louisville and the other Pacific hot spots that was not corrected for in the global S04G model. Finally, based on six new $^{40}Ar/^{39}Ar$ age dates, the 169°W bend in the Louisville seamount trail seems to have formed at least 3 Myr before the formation of the Hawaiian-Emperor bend. The timing of the most acute parts of both bends thus appears to be asynchronous, which would require other processes (e.g., plume motions) than a global plate motion change between 50 and 47 Ma to explain these two observations.

Components: 13,200 words, 9 figures, 2 tables.

Keywords: $^{40}Ar/^{39}Ar$ geochronology; Pacific plate; guyots; hot spots; seamounts; submarine alteration.

Index Terms: 8137 Tectonophysics: Hotspots, large igneous provinces, and flood basalt volcanism; 8157 Tectonophysics: Plate motions: past (3040); 8415 Volcanology: Intra-plate processes (1033, 3615).

Received 19 July 2011; **Revised** 8 November 2011; **Accepted** 10 November 2011; **Published** 30 December 2011.

Koppers, A. A. P., M. D. Gowen, L. E. Colwell, J. S. Gee, P. F. Lonsdale, J. J. Mahoney, and R. A. Duncan (2011), New $^{40}Ar/^{39}Ar$ age progression for the Louisville hot spot trail and implications for inter–hot spot motion, *Geochem. Geophys. Geosyst.*, *12*, Q0AM02, doi:10.1029/2011GC003804.

Theme: Studies of Seamount Trials: Implications for Geodynamic Mantle Flow Models and the Geochemical Evolution of Primary Hot Spots

1. Introduction

[2] Seamount trails are purported to form when hot, buoyant material rises from the (deep) mantle and partially melts due to decompression beneath the oceanic lithosphere. Once the melt reaches the surface, a volcanic trail of ocean islands and seamounts is created as the tectonic plate moves over the hot spot. The original hypothesis explained hot spots [*Wilson*, 1963] by assuming the presence of narrow plumes upwelling from a fixed position in the deep mantle, providing a stationary long-term reference frame within which past plate motions could be determined [*Morgan*, 1972]. Under this attractive working hypothesis, absolute plate motion (APM) models for every tectonic plate on Earth could then be determined. The latest of these APM models for the Pacific plate (W06, WK08G and WK08H [*Wessel et al.*, 2006; *Wessel and Kroenke*, 2008]) combine ages and seamount trail morphologies to derive plate motions, based on the premise that *all* hot spots in the Pacific (and their underlying mantle plumes) have remained fixed for the past 145 million years.

[3] Over the last decades, modifications of the Wilson-Morgan hot spot hypothesis have been required, while other researchers have rejected the model and advocate a complete rethinking of the processes that may cause intraplate volcanism (see *Koppers and Watts* [2010] for a review). The most severe modification "unfixed" the plumes in the Earth's (deep) mantle, and from the sparse data set we have at present, it seems very plausible that some plumes move at speeds not much different from the velocities of the tectonic plates; that is, at rates of up to 50 mm/year [*Tarduno et al.*, 2003]. Geodynamical modeling now also shows mantle plumes to be decidedly more mobile [*Steinberger*, 2000; *Steinberger and O'Connell*, 1998] and mantle convection even somewhat chaotic [*Davies and Davies*, 2009; *Lin and van Keken*, 2006]. A more serious problem is caused by the often complex and sometimes complete absence of unambiguous age progressions in many of the studied seamount trails that characteristically are not much longer lived than 30 million years [*Koppers and Staudigel*, 2005; *Koppers et al.*, 2007, 2003b]. Another complexity arises from the fact that the bends in the orientation of seamount trails, such as the Hawaiian-Emperor bend, may not have formed at the same time for some of the Pacific seamount trails [*Koppers and Staudigel*, 2005], whereas the Wilson-Morgan hypothesis clearly demands synchronicity in the timing of these bends. Finally, plate circuit modeling and transferring of, for example, Indo-Atlantic plate–hot spot motions to Pacific plate–Hawaiian hot spot motion have shown consistent discrepancies with observed volcanic trails, in particular prior to 40 Ma [*Cande et al.*, 1995; *Doubrovine and Tarduno*, 2008a, 2008b; *Raymond et al.*, 2000]. The lack of linear age progressions, the asynchronous timing of seamount

trail bends, and the misfit between global hot spot systems in plate circuit models, often are cited as reasons that the original Wilson-Morgan hypothesis is flawed or needs an overhaul [*Foulger*, 2007; *Foulger and Natland*, 2003].

[4] The two seamount trails that generate fewer objections are those related to the Hawaiian and Louisville hot spots. These two systems are regarded as key examples of primary hot spots [*Courtillot et al.*, 2003] and their age progressive volcanic trails and apparently synchronous bends seem generally compatible with the Wilson-Morgan hot spot hypothesis. Both systems are long-lived at ~80 Myr and have produced more or less continuous volcanism over their life spans. By measuring the ages of a sufficient number of seamounts and the distances (great circle) between these two hot spots over time, a record of differential motion can be established [*Wessel and Kroenke*, 2009]. We can also compare the seamount age distributions to predictions from APM models that assume fixed hot spots [e.g., *Duncan and Clague*, 1985; *Koppers et al.*, 2001; *Wessel et al.*, 2006; *Wessel and Kroenke*, 1997, 2008]. If mantle plumes are indeed stationary with respect to one another, this exercise should reveal no differential motion over their volcanic histories and age distributions, consistent with the APM models. In that case, the morphological and temporal evolution of both the Hawaiian and Louisville volcanic systems should be similar and completely controlled by changes in the past motion of the Pacific plate. Alternatively, we can compare the age progressions with APM models that allow for hot spot motions [e.g., *Steinberger et al.*, 2004]. If these advanced APM models are a better fit to the observed age progressions in Hawaii and Louisville, and if significant changes in their inter–hot spot distances are revealed, it is likely that these two hot spots have experienced independent motion histories.

[5] The alternative approach arguably is the most promising, because the mantle plume theory does not require stationary hot spots [e.g., *Cande et al.*, 1995; *Koppers et al.*, 2001] and because paleomagnetic study of samples from four Emperor seamounts has shown that the Hawaiian hot spot moved 15° south between 80 and 50 Ma [*Kono*, 1980; *Tarduno et al.*, 2009, 2003]. Mantle flow models now also indicate that the Louisville hot spot might have moved, although in quite a different direction and not as far. Depending on assumptions made in these mantle flow models, the Louisville hot spot may have moved eastward over the last 120 Myr, with a maximum shift in paleolatitude of merely 2 to 6 degrees between 80 Ma and the present-day [*Koppers et al.*, 2004; *Steinberger and Antretter*, 2006; *Steinberger and Calderwood*, 2006; *Steinberger et al.*, 2004]. This should be resolvable from the 15° paleolatitude shift observed during the same time period in the Hawaiian-Emperor seamount trail [*Koppers et al.*, 2010b]. Remarkably, inter–hot spot distances between these two seamount trails have been rather constant for the younger portions of the trails, yet these distances increase significantly prior to 55 Ma [*Wessel and Kroenke*, 2009]. Thus, under the assumption of a rigid Pacific plate, only a small amount of differential motion between Hawaiian and Louisville hot spots is allowable over the last 55 Myr, yet for earlier Cretaceous times a more significant amount of inter–hot spot motion still needs to be considered.

[6] In this paper we present new $^{40}Ar/^{39}Ar$ ages for the Louisville seamount trail (Figure 1) that provide evidence for an age-progressive trend, departing from that of the Hawaiian-Emperor trail and APM models. From ~21 Ma toward the older end of the Louisville seamount trail, the Louisville seamount ages are older than the most recent APM model predictions (assuming fixed hot spots) and measured ages of congruent Hawaiian seamounts, with offsets ranging up to 6 Myr. We show that this is most likely the result of past differential motion between the Louisville and Hawaii hot spots. However, we also consider other mechanisms that may have caused the 6 Myr offsets in the Louisville seamount ages. For example, the presumed present-day location of the Louisville hot spot may have been misplaced in existing APM models and we will show here that the fit to these models can be improved by placing it farther east and closer to the spreading center at the Pacific-Antarctic Ridge. The current (large) database of Louisville ages also may be biased to younger ages, if dredging of the Louisville seamounts sampled late-stage lava flows only. Uncertainty about the magmatic progression and duration of the investigated Louisville volcanoes [*Koppers et al.*, 2010b] adds ambiguity to our interpretations, even though it is clear that the potential recovery of older volcanic stages at the Louisville seamounts will make the age offsets even larger.

2. Geological Setting

[7] The Louisville seamount trail stretches 4,300 km and is positioned to the southeast of Samoa and east of the Tonga Trench (Figure 1). It is a narrow, ~75 km wide chain of mainly guyots and some smaller seamounts, yet its volcanic output is an

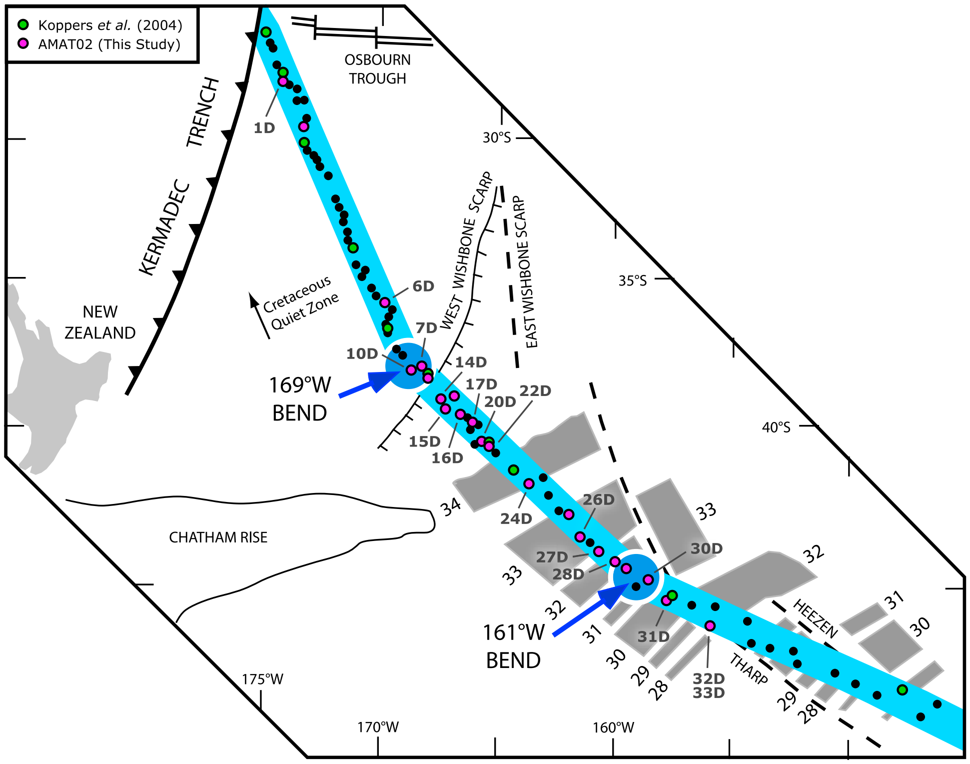

Figure 1. Overview map and sampling locations along the Louisville seamount trail. Only locations for samples dated using the $^{40}Ar/^{39}Ar$ geochronology technique are indicated, from the study by *Koppers et al.* [2004] and this study that is entirely based on basalts collected during the AMAT02 site survey for IODP Expedition 330 [*Koppers et al.*, 2010b].

order of magnitude lower than that of Hawaii and diminishes almost entirely toward its young (eastern) end [*Lonsdale*, 1988]. For this reason, the present-day location and even the continued existence of the Louisville hot spot is uncertain. It seems that all Louisville volcanoes have been erupted onto seafloor that was about 40–50 Myr old [*Lonsdale*, 1988; *Watts et al.*, 1988]. This is well established for the young end of the trail, which is positioned on top of early Tertiary (Chron 25–33) oceanic crust, but its oldest (northwestern) portion formed on oceanic crust that was produced during the Cretaceous normal superchron and close to the Osbourn Trough, a former mid-ocean spreading center [*Downey et al.*, 2007]. Three-dimensional flexural studies of various Louisville seamounts [*Lyons et al.*, 2000] suggest that the underlying ocean crust indeed is about 40–50 Myr older, yet a recent seismic refraction experiment provided a direct image of the downward-flexed Moho underneath one of the oldest Louisville seamounts (~76 Ma) which can be explained only if this seamount was emplaced upon oceanic lithosphere ~10 Myr old [*Contreras-Reyes et al.*, 2010]. This latter outcome is in agreement with the ocean crust age model for the Louisville seamount trail region presented in the global compilation of magnetic isochrons that went into *Müller et al.*'s [2008] map. The oldest extant seamount in the trail is Osbourn Guyot (77–79 Ma) [*Koppers et al.*, 2004] which is just entering the Tonga trench with the leading edge of the Pacific plate. Older seamounts in this trail have already been subducted [*Ballance et al.*, 1989] as confirmed by geochemical evidence from volcanoes in the Tonga Arc [*Regelous et al.*, 1997; *Turner and Hawkesworth*, 1997].

[8] The Louisville seamounts lineament is regarded by many as one of the type examples of a hot spot trail and has been designated a primary hot spot trail because of its linear age progression and long-continued volcanic output [*Courtillot et al.*, 2003]. However, from a geochemical point of view, the Louisville seamount trail is quite different from the better-known Hawaiian-Emperor primary hot spot trail. None of the more than 70 dredge hauls that collected volcanic rocks along the Louisville seamount trail [e.g., *Hawkins et al.*, 1987; *Vanderkluysen et al.*, 2007] have included tholeiitic lavas, a dominant rock type along the Hawaiian-Emperor seamount trail, and radiogenic isotope ratios measured are much

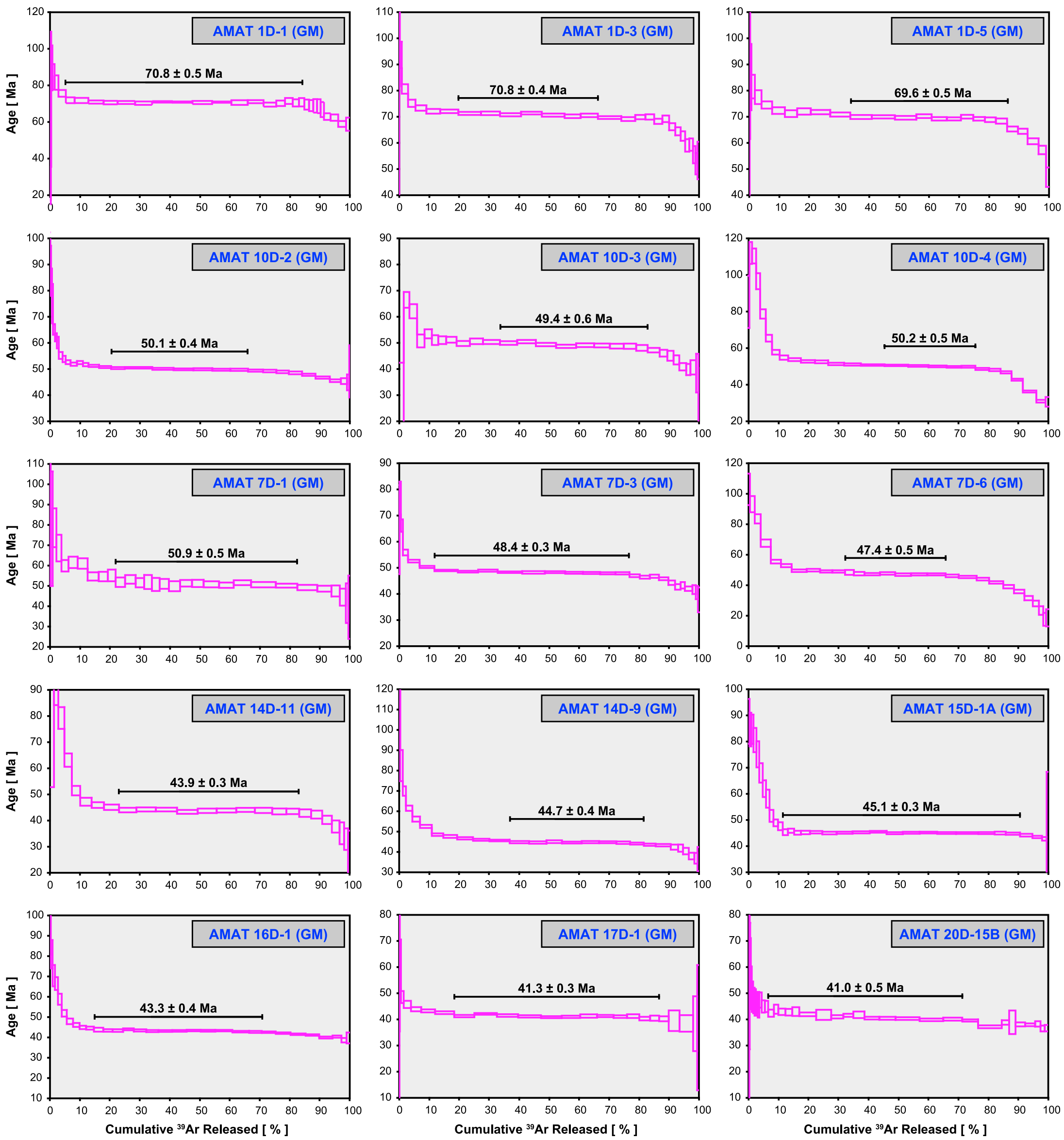

Figure 2. High-resolution incremental heating $^{40}Ar/^{39}Ar$ age spectra for Louisville seamount trail basalts collected during AMAT02 site survey. The age spectra are presented from old to young along the seamount trail. The $^{40}Ar/^{39}Ar$ ages are weighted age estimates with errors reported at the 95% confidence level, including 0.3–0.5% standard deviations in the J-value. All samples were monitored against FCT-3 biotite (28.03 ± 0.18 Ma, 1σ) as calibrated by *Renne et al.* [1998]. Data are listed in Table 2 and ArArCALC age calculation files can be downloaded from the EarthRef.org Digital Archive (ERDA) as described in Text S1.

more uniform than in Hawaiian lavas [*Beier et al.*, 2011; *Cheng et al.*, 1987; *Vanderkluysen et al.*, 2007]. It thus is plausible that typical Louisville volcanoes have eruptive histories that are significantly different from the volcanoes in the Hawaiian-Emperor seamount trail. However, it remains possible that Louisville volcanoes have tholeittic shields buried beneath the alkali carapaces as sampled by dredging, but this is less likely following the almost exclusive recovery of alkalic lavas during IODP Expedition 330 from drill holes as deep as 522 mbsf [*Expedition 330 Scientists*, 2011].

3. Sampling and $^{40}Ar/^{39}Ar$ Dating Techniques

[9] In 2006, the AMAT02 Expedition of the R/V Roger Revelle mapped and dredged 72 Louisville guyots and seamounts and collected multichannel seismic reflection data in preparation for IODP

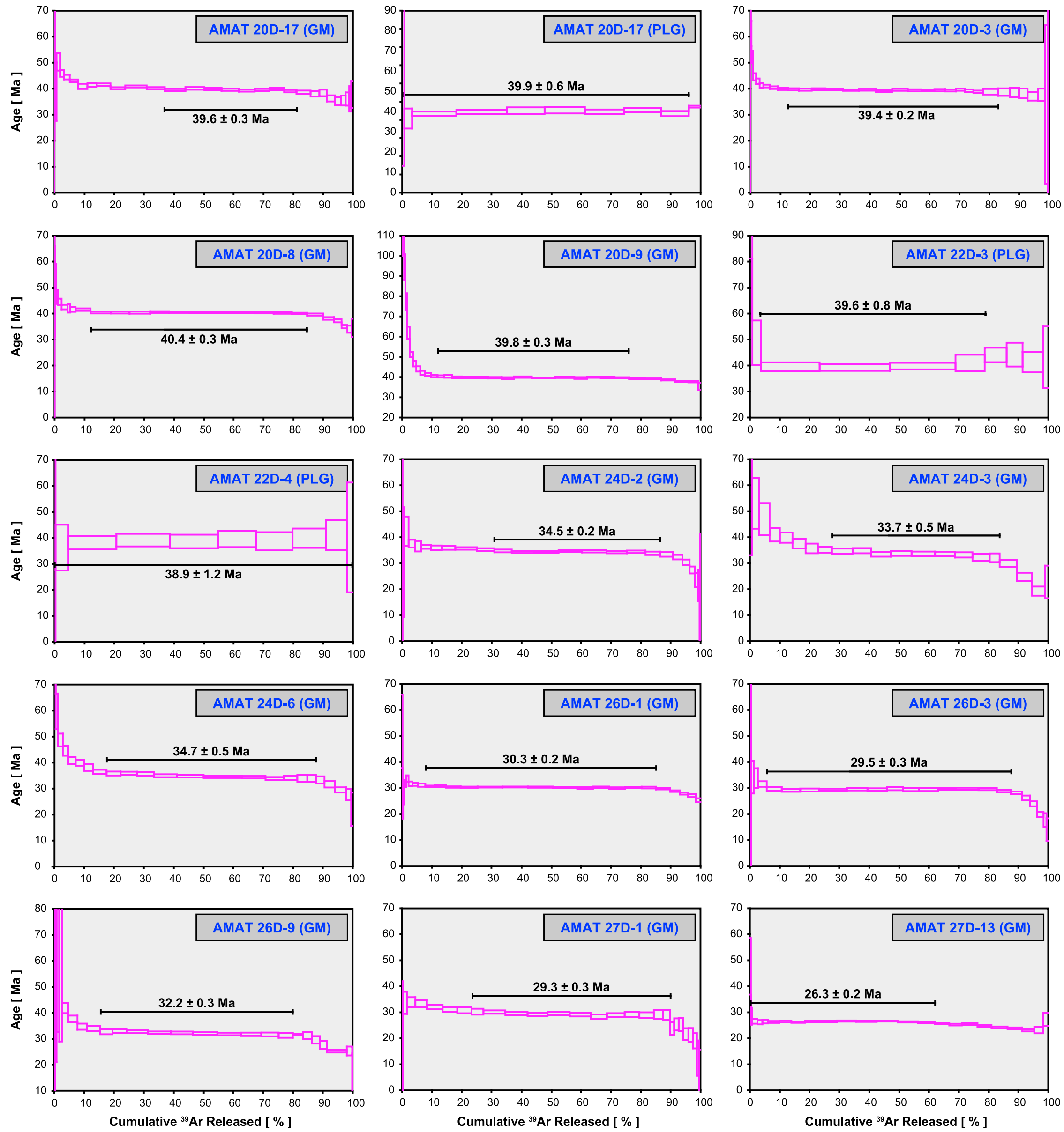

Figure 2. (continued)

Expedition 330 [*Koppers et al.*, 2010b]. Out of a total of 29 successful dredge hauls, 19 dredges from 17 seamounts provided suitable samples for this study. In total, we performed 46 new $^{40}Ar/^{39}Ar$ incremental heating analyses for these seamounts along the middle 2/3 of the Louisville seamount trail, which vary in age between 21 and 71 Ma. For 42 successful analyses, which yielded estimates of the seamount eruption ages, detailed incremental heating experiments are displayed in Figure 2. Seamount locations and a summary of the $^{40}Ar/^{39}Ar$ ages are listed in Tables 1 and 2 and plotted on the bathymetric maps in Figure 3. Measurement data and the ArArCALC age calculation files (in PDF format) can be downloaded from the EarthRef.org Digital Archive (ERDA; as detailed in Text S1) and are also provided in the auxiliary material.[1]

3.1. Sample Preparation and Acid Leaching

[10] The majority of samples analyzed were groundmass separates prepared from aphyric basalts. In five

[1]Auxiliary materials are available in the HTML. doi:10.1029/2011GC003804.

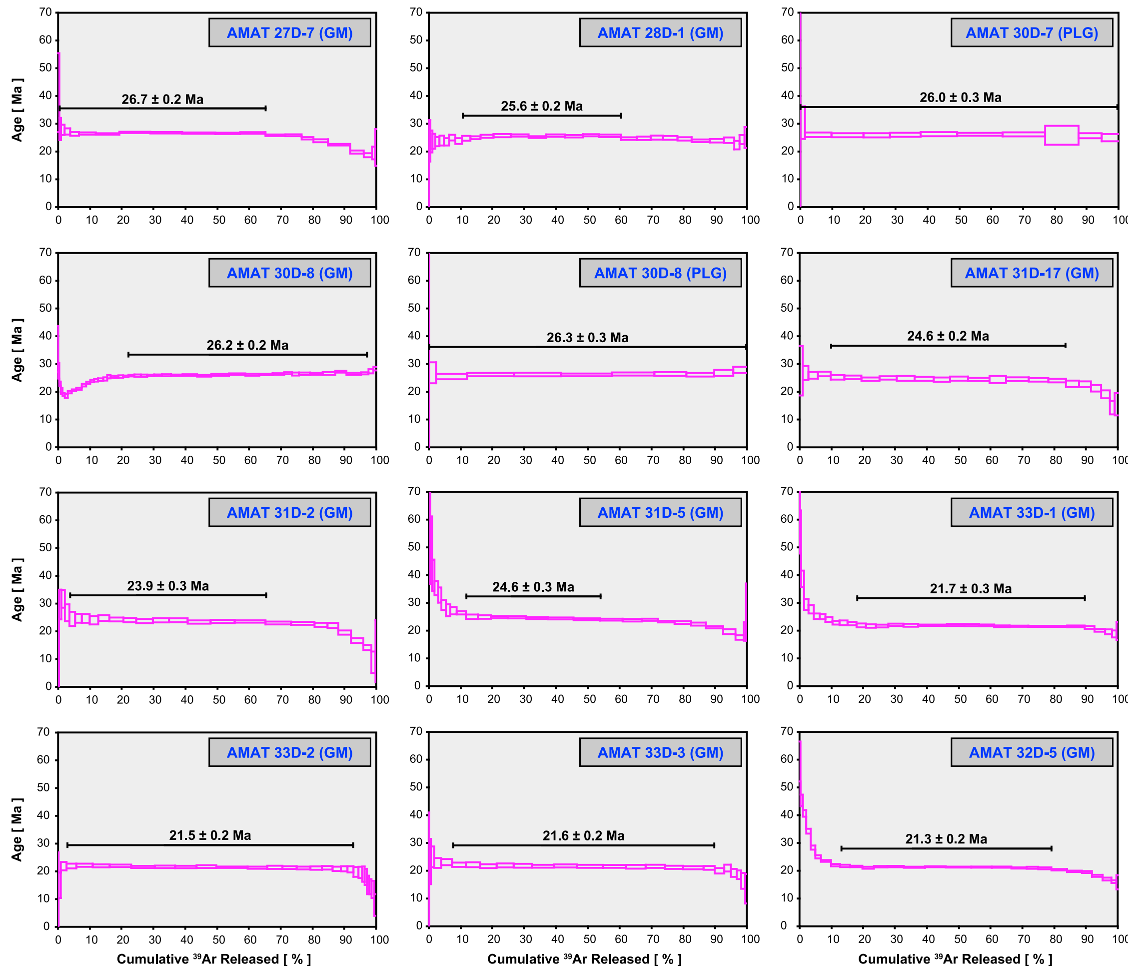

Figure 2. (continued)

cases we could separate plagioclase, which we then analyzed to assess the age reproducibility and accuracy of the groundmass $^{40}Ar/^{39}Ar$ age analyses within the same dredge haul (AMAT 20D, 22D and 30D) or the same sample (AMAT 20D-17 and 30D-8). Visibly obvious alteration was removed from the groundmass samples by using a rock saw. This was followed by crushing the samples using a porcelain jaw crusher, stainless steel ring mill and in some cases a porcelain hand mortar until approximately 25% of the grains were sieved into the 210–300 μm fraction. This size fraction was rinsed several times using ultra-pure de-ionized water and set in a 40°C oven to dry overnight. Some groundmass samples were further processed using a Frantz magnetic separator to remove the non-magnetic (and often more altered) fraction. Finally, all samples were cleaned by acid leaching in 1N HCl (60 min), 6N HCl (60 min), 1N HNO3 (60 min) and ultra-pure de-ionized water (60 min) in an ultrasonic bath heated to ~50°C. Before irradiation, approximately 100 mg of groundmass was hand-picked for each sample using a binocular microscope to remove any grains containing (remaining) alteration or larger parts of mafic phenocrysts and microcrysts that can be sources of excess mantle-derived ^{40}Ar. Plagioclase samples were prepared in the same way except that the acid leaching included an extra step with 5% HF (15 min) to gently etch away the (altered) rims of the plagioclase crystals. Approximately 50 mg of plagioclase was separated from each sample.

3.2. $^{40}Ar/^{39}Ar$ Mass Spectrometry and Age Calculations

[11] The groundmass and plagioclase samples were irradiated for 7–10 h in the TRIGA CLICIT nuclear reactor at Oregon State University, along with the FCT-3 biotite (28.03 ± 0.18 Ma, 1σ) flux monitor [*Renne et al.*, 1998]. Individual J-values for each sample were calculated by parabolic extrapolation of the measured flux gradient against irradiation height and typically give 0.3–0.5% uncertainties

Table 1. Sample Locations in the Louisville Seamount Trail[a]

Sample	Laboratory Code	Seamount	Latitude	Longitude	Depth (mbsf)	Distance Hot Spot (deg.)
AMAT 1D-1	LOU-11	27.6°S (Volcano 33)	27°30.9′S	174°20.6′W	2472–2100	37.671
AMAT 1D-3	LOU-12	27.6°S (Volcano 33)	27°30.9′S	174°20.6′W	2472–2100	37.671
AMAT 1D-5	LOU-13	27.6°S (Volcano 33)	27°30.9′S	174°20.6′W	2472–2100	37.671
AMAT 6D-2	LOU-14	35.8°S	35°50.6′S	169°53.9′W	2067–1650	28.536
AMAT 6D-3	LOU-15	35.8°S	35°50.6′S	169°53.9′W	2067–1650	28.536
AMAT 10D-2	LOU-19	168.6°W	38°10.3′S	168°39.6′W	1535–1258	26.012
AMAT 10D-3	LOU-20	168.6°W	38°10.3′S	168°39.6′W	1535–1258	26.012
AMAT 10D-4	LOU-21	168.6°W	38°10.3′S	168°39.6′W	1535–1258	26.012
AMAT 7D-1	LOU-16	168.3°W	38°02.3′S	168°15.9′W	1950–1605	25.898
AMAT 7D-3	LOU-17	168.3°W	38°02.3′S	168°15.9′W	1950–1605	25.898
AMAT 7D-6	LOU-18	168.3°W	38°02.3′S	168°15.9′W	1950–1605	25.898
AMAT 14D-11	LOU-23	167.4°W	39°13.1′S	167°37.1′W	2335–1910	24.696
AMAT 14D-9	LOU-22	167.4°W	39°13.1′S	167°37.1′W	2335–1910	24.696
AMAT 15D-1a	LOU-24	167.3°W	39°31.2′S	167°15.3′W	2318–1852	24.284
AMAT 16D-1	LOU-25	166.6°W	39°40.6′S	166°38.6′W	2462–2117	23.839
AMAT 17D-1	LOU-26	166.1°W	39°51.9′S	166°02.7′W	2439–1996	23.385
AMAT 20D-15B	LOU-32	165.7°W	40°26.7′S	165°44.4′W	2179–1880	22.807
AMAT 20D-17	LOU-33	165.7°W	40°26.7′S	165°44.4′W	2179–1880	22.807
AMAT 20D-17	LOU-33	165.7°W	40°26.7′S	165°44.4′W	2179–1880	22.807
AMAT 20D-3	LOU-28	165.7°W	40°26.7′S	165°44.4′W	2179–1880	22.807
AMAT 20D-8	LOU-30	165.7°W	40°26.7′S	165°44.4′W	2179–1880	22.807
AMAT 20D-9	LOU-31	165.7°W	40°26.7′S	165°44.4′W	2179–1880	22.807
AMAT 19D-1	LOU-27	165.7°W	40°25.7′S	165°41.1′W	1262–1062	22.790
AMAT 22D-3	LOU-35	165.4°W	40°44.5′S	165°27.6′W	1899–1831	22.448
AMAT 22D-4	LOU-36	165.4°W	40°44.5′S	165°27.6′W	1899–1831	22.448
AMAT 24D-2	LOU-37	163.6°W	41°52.7′S	163°41.9′W	1390–1115	20.706
AMAT 24D-3	LOU-38	163.6°W	41°52.7′S	163°41.9′W	1390–1115	20.706
AMAT 24D-6	LOU-39	163.6°W	41°52.7′S	163°41.9′W	1390–1115	20.706
AMAT 26D-1	LOU-40	161.5°W	43°34.5′S	161°29.3′W	1514–1224	18.377
AMAT 26D-3	LOU-41	161.5°W	43°34.5′S	161°29.3′W	1514–1224	18.377
AMAT 26D-7	LOU-42	161.5°W	43°34.5′S	161°29.3′W	1514–1224	18.377
AMAT 26D-9	LOU-43	161.5°W	43°34.5′S	161°29.3′W	1514–1224	18.377
AMAT 27D-1	LOU-44	160.7°W	43°59.7′S	160°37.1′W	1435–1174	17.617
AMAT 27D-13	LOU-46	160.7°W	43°59.7′S	160°37.1′W	1435–1174	17.617
AMAT 27D-7	LOU-45	160.7°W	43°59.7′S	160°37.1′W	1435–1174	17.617
AMAT 28D-1	LOU-47	159.8°W	44°16.5′S	159°48.9′W	1685–1320	16.988
AMAT 30D-7	LOU-48	158.5°W	44°50.6′S	158°28.4′W	1504–1225	15.881
AMAT 30D-8	LOU-49	158.5°W	44°50.6′S	158°28.4′W	1504–1225	15.881
AMAT 30D-8	LOU-49	158.5°W	44°50.6′S	158°28.4′W	1504–1225	15.881
AMAT 31D-17	LOU-52	157.7°W	45°22.9′S	157°44.0′W	1560–1227	15.142
AMAT 31D-2	LOU-50	157.7°W	45°22.9′S	157°44.0′W	1560–1227	15.142
AMAT 31D-5	LOU-51	157.7°W	45°22.9′S	157°44.0′W	1560–1227	15.142
AMAT 33D-1	LOU-54	155.9°W (Rumyantsev)	46°13.2′S	155°52.7′W	1128–948	13.602
AMAT 33D-2	LOU-55	155.9°W (Rumyantsev)	46°13.2′S	155°52.7′W	1128–948	13.602
AMAT 33D-3	LOU-56	155.9°W (Rumyantsev)	46°13.2′S	155°52.7′W	1128–948	13.602
AMAT 32D-5	LOU-53	155.9°W (Rumyantsev)	46°13.6′S	155°52.8′W	1369–1101	13.599

[a]The samples used in this study were dredged in 2006 during the AMAT02 site survey expedition using the R/V Roger Revelle.

(1σ). The $^{40}Ar/^{39}Ar$ incremental heating age determinations were performed using a continuous 10W CO_2 laserprobe combined with a MAP-215/50 mass spectrometer at Oregon State University. Irradiated samples were loaded into Cu-planchettes in an ultra-high vacuum sample chamber and incrementally heated by scanning a defocused CO_2 laser beam in preset patterns across the sample in order to evenly release the argon gas. After heating, reactive gases were cleaned up using an SAES Zr-Al ST101 GP50 getter operated at 400°C for ~15 min and two SAES Fe-V-Zr ST172 getters operated at 200°C and room temperature, respectively. Before analyzing a sample, and after every three heating steps, system blanks were measured. Data peak intensities were reduced using linear or exponential curve fits

Table 2. Incremental Heating $^{40}Ar/^{39}Ar$ Analyses on the Louisville Seamount Trail[a]

				Age Spectrum						Total Fusion		Inverse Isochron Analyses		
Sample	Laboratory Code	Experiment	Sample Type	Age ± 2σ (Ma)	^{39}Ar (%)	K/Ca	MSWD	n	N	Age ± 2σ (Ma)	K/Ca	Age ± 2σ (Ma)	$^{40}Ar/^{36}Ar$ Intercept	MSWD
AMAT 1D-1	LOU-11	08C2630	Groundmass	70.8 ± 0.4	79	0.293	0.89	17	32	70.2 ± 0.4	0.147			
AMAT 1D-3	LOU-12	08C2072	Groundmass	70.8 ± 0.4	47	0.241	2.21	7	29	70.2 ± 0.3	0.127			
AMAT 1D-5	LOU-13	08C2520	Groundmass	69.6 ± 0.5	52	0.218	2.18	10	26	69.5 ± 0.4	0.130			
AMAT 6D-2	LOU-14	08C2555	Groundmass	too altered	too altered	too altered								
AMAT 6D-3	LOU-15	08C2226	Groundmass	too altered	too altered	too altered								
AMAT 10D-2	LOU-19	07C3871	Groundmass	50.1 ± 0.4	47	0.387	2.88	7	32	50.3 ± 0.4	0.243			
AMAT 10D-3	LOU-20	08C2480	Groundmass	49.4 ± 0.6	49	0.204	3.64	9	29	49.0 ± 0.4	0.211			
AMAT 10D-4	LOU-21	08C4541	Groundmass	50.2 ± 0.5	30	0.146	2.36	5	26	52.1 ± 0.4	0.132			
AMAT 7D-1	LOU-16	07C3913	Groundmass	50.9 ± 0.5	61	0.092	0.92	14	30	52.6 ± 0.6	0.047	50.4 ± 0.4	309.6 ± 6.3	0.54
AMAT 7D-3	LOU-17	08C2190	Groundmass	48.4 ± 0.3	65	0.290	4.67	10	27	48.1 ± 0.2	0.158			
AMAT 7D-6	LOU-18	08C4612	Groundmass	47.4 ± 0.5	34	0.111	0.75	7	28	47.8 ± 0.4	0.073			
AMAT 14D-11	LOU-23	08C2597	Groundmass	43.9 ± 0.3	60	0.118	0.63	10	25	45.8 ± 0.4	0.077			
AMAT 14D-9	LOU-22	07C3753	Groundmass	44.7 ± 0.4	45	0.142	0.97	8	27	46.6 ± 0.4	0.099			
AMAT 15D-1a	LOU-24	07C3711	Groundmass	45.1 ± 0.3	79	0.215	0.92	17	32	47.2 ± 0.4	0.188	45.1 ± 0.3	310.3 ± 9.7	0.81
AMAT 16D-1	LOU-25	07C3830	Groundmass	43.3 ± 0.4	56	0.212	1.96	13	31	44.0 ± 0.3	0.135			
AMAT 17D-1	LOU-26	08C2673	Groundmass	41.3 ± 0.3	68	0.213	4.16	12	25	41.5 ± 0.4	0.136			
AMAT 20D-15B	LOU-32	09C2830	Groundmass	41.0 ± 0.5	65	0.378	6.68	15	39	40.8 ± 0.3	0.166			
AMAT 20D-17	LOU-33	08C2031	Groundmass	39.6 ± 0.3	44	0.297	2.30	8	31	40.0 ± 0.2	0.148			
AMAT 20D-17	LOU-33	07C4180	Plagioclase	39.9 ± 0.6	96	0.014	1.39	9	10	40.1 ± 0.6	0.013	39.9 ± 0.3	299.0 ± 7.3	1.54
AMAT 20D-3	LOU-28	08C2149	Groundmass	39.4 ± 0.2	70	0.314	1.95	16	33	39.4 ± 0.5	0.163			
AMAT 20D-8	LOU-30	08C4178	Groundmass	40.4 ± 0.3	73	0.363	0.92	11	26	40.3 ± 0.3	0.192			
AMAT 20D-9	LOU-31	07C3788	Groundmass	39.8 ± 0.3	64	0.457	1.51	14	32	41.1 ± 0.3	0.300			
AMAT 19D-1	LOU-27	08C4032	Groundmass	too altered	too altered	too altered								
AMAT 22D-3	LOU-35	07C4151	Plagioclase	39.6 ± 0.8	75	0.009	0.38	4	10	41.4 ± 0.9	0.009	39.5 ± 0.5	332.8 ± 43	0.54
AMAT 22D-4	LOU-36	09C2915	Plagioclase	38.9 ± 1.2	100	0.008	0.22	10	10	39.1 ± 1.3	0.008			
AMAT 24D-2	LOU-37	08C4073	Groundmass	34.5 ± 0.2	56	0.135	1.20	8	26	34.5 ± 0.3	0.111			

Table 2. (continued)

Sample	Laboratory Code	Experiment	Sample Type	Age Spectrum: Age ± 2σ (Ma)	^{39}Ar (%)	K/Ca	MSWD	n	N	Total Fusion: Age ± 2σ (Ma)	K/Ca	Inverse Isochron Analyses: Age ± 2σ (Ma)	^{40}Ar/^{36}Ar Intercept	MSWD
AMAT 24D-3	LOU-38	08C3021	Groundmass	33.7 ± 0.5	56	0.070	2.14	9	21	34.2 ± 0.5	0.058			
AMAT 24D-6	LOU-39	07C4282	Groundmass	34.7 ± 0.5	70	0.120	4.66	11	24	36.1 ± 0.4	0.095			
AMAT 26D-1	LOU-40	07C4081	Groundmass	30.3 ± 0.2	77	0.412	1.91	13	26	30.1 ± 0.2	0.216			
AMAT 26D-3	LOU-41	08C5028	Groundmass	29.5 ± 0.3	82	0.163	1.17	13	23	28.9 ± 0.4	0.128	29.5 ± 0.3	292.3 ± 8.6	1.26
AMAT 26D-7	LOU-42	09C2881	Groundmass	too altered	too altered	too altered								
AMAT 26D-9	LOU-43	08C2987	Groundmass	32.2 ± 0.3	65	0.185	2.20	10	25	32.6 ± 0.5	0.196			
AMAT 27D-1	LOU-44	08C4110	Groundmass	29.3 ± 0.3	67	0.112	1.67	12	27	29.1 ± 0.3	0.098			
AMAT 27D-13	LOU-46	07C4216	Groundmass	26.3 ± 0.2	62	0.508	1.66	14	24	25.7 ± 0.2	0.243	26.3 ± 0.2	296.1 ± 3.5	1.80
AMAT 27D-7	LOU-45	07C4313	Groundmass	26.7 ± 0.2	65	0.276	1.78	11	21	25.6 ± 0.2	0.157	26.6 ± 0.2	299.7 ± 5.9	1.87
AMAT 28D-1	LOU-47	08C2947	Groundmass	25.6 ± 0.2	50	0.288	2.06	10	30	24.9 ± 0.2	0.175			
AMAT 30D-7	LOU-48	09C2929	Plagioclase	26.0 ± 0.3	100	0.032	0.66	11	12	26.1 ± 0.5	0.032	25.8 ± 0.3	325.2 ± 23	0.53
AMAT 30D-8	LOU-49	07C3986	Groundmass	26.2 ± 0.2	75	2.000	4.77	22	44	25.6 ± 0.2	2.140	25.4 ± 0.2	317.9 ± 3.6	1.58
AMAT 30D-8	LOU-49	07C4165	Plagioclase	26.3 ± 0.3	100	0.041	1.38	10	11	26.4 ± 0.3	0.042	26.4 ± 0.5	292.1 ± 12	1.54
AMAT 31D-17	LOU-52	08C4145	Groundmass	24.6 ± 0.2	74	0.144	1.03	13	26	24.2 ± 0.2	0.094			
AMAT 31D-2	LOU-50	08C4507	Groundmass	23.9 ± 0.3	62	0.171	1.14	13	23	22.9 ± 0.2	0.099	23.7 ± 0.2	311.5 ± 7.9	0.83
AMAT 31D-5	LOU-51	07C4246	Groundmass	24.6 ± 0.3	42	0.153	2.33	7	27	24.7 ± 0.3	0.098	24.2 ± 0.2	367.6 ± 28	0.91
AMAT 33D-1	LOU-54	07C4044	Groundmass	21.7 ± 0.3	72	0.239	1.78	13	29	22.4 ± 0.3	0.160	21.6 ± 0.2	357.3 ± 45	1.61
AMAT 33D-2	LOU-55	08C2110	Groundmass	21.5 ± 0.2	90	0.180	1.56	18	29	21.1 ± 0.2	0.130	21.2 ± 0.1	383.8 ± 29	0.73
AMAT 33D-3	LOU-56	08C4578	Groundmass	21.6 ± 0.2	83	0.196	1.00	14	25	21.5 ± 0.2	0.115			
AMAT 32D-5	LOU-53	07C4115	Groundmass	21.3 ± 0.2	66	0.462	2.50	13	28	21.7 ± 0.2	0.240			

[a]K/Ca values are calculated as weighted means for the age spectra or as total fusion K/Ca values by combining the gas analyses. Both the number of steps (n) included in the age plateau and isochron calculations and the total number of incremental heating steps (N) have been listed. MSWD values for the age plateaus and inverse isochrons are calculated using n-1 and n-2 degrees of freedom, respectively. All samples from this study where monitored against FCT-3 biotite (28.03 ± 0.18 Ma) as calibrated by *Renne et al.* [1998]. Reported errors on the ^{40}Ar/^{39}Ar ages are at the 95% confidence level (2σ) including 0.3–0.4% standard deviation in the J-value. All input parameters to the calculations are published in Table 2 of *Koppers et al.* [2003a]. Due to the intensive acid-leaching of the groundmass samples dated, the atmospheric component (from alteration, absorption and trapped argon) in some cases may have been effectively removed, resulting in extremely high radiogenic components for the age plateaus and a clustering of the data points near the intercept on the ^{39}Ar/^{40}Ar axis. Whenever the radiogenic components for all steps included in the age calculations are higher than 95% we consider these data points "too radiogenic" to calculate meaningful isochrons and thus these data have not be listed.

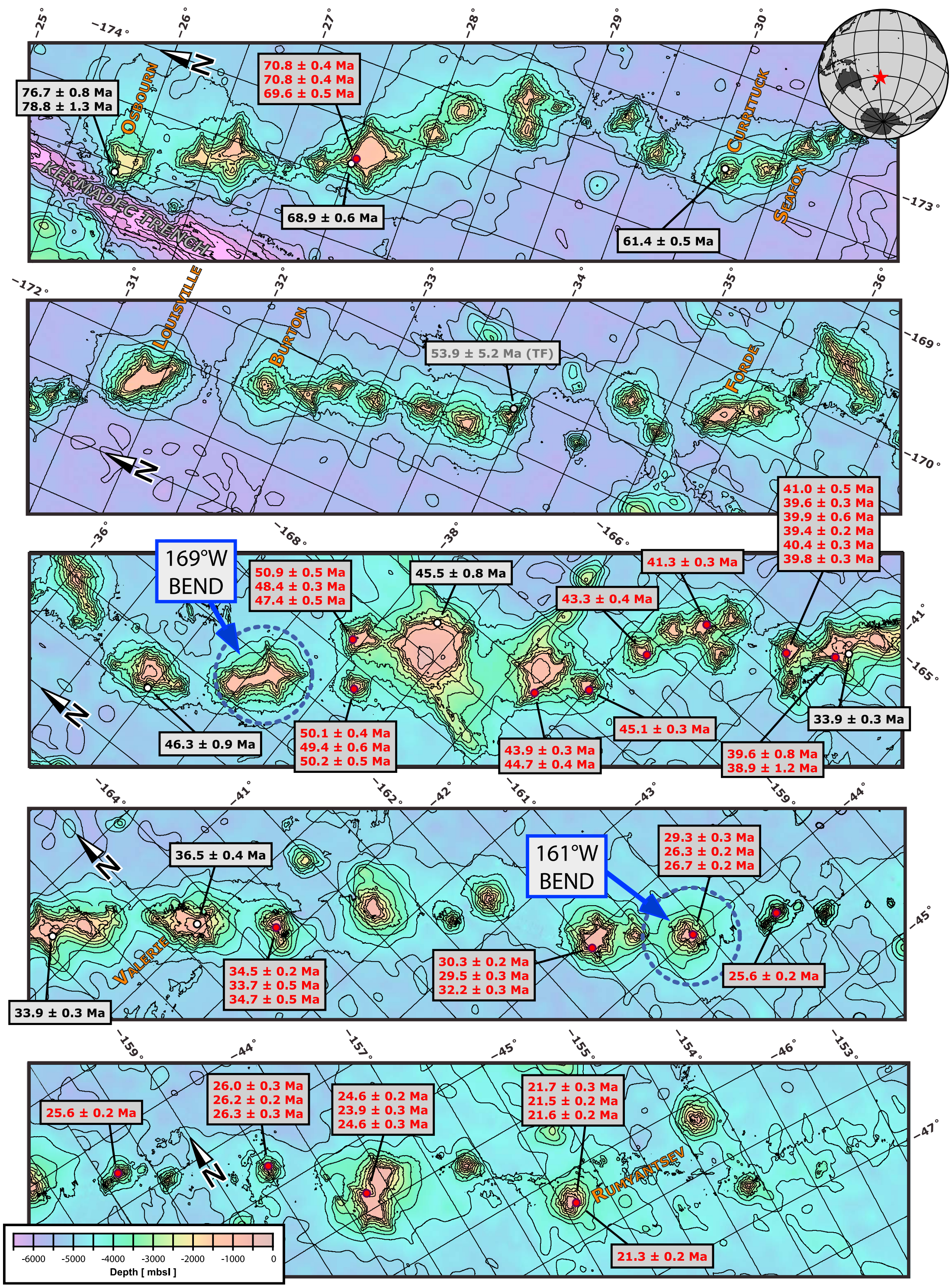

Figure 3. Bathymetric maps of the Louisville seamounts with measured $^{40}Ar/^{39}Ar$ ages (in Ma). The bathymetric maps are based on a combination of SIMRAD EM120 multibeam data collected during the AMAT02 site survey expedition onboard the R/V Roger Revelle and are merged with the global predicted bathymetry (v8.2) from *Smith and Sandwell* [1997]. Ages are from *Koppers et al.* [2004] (black font), this study (red font) and one is a less precise total fusion $^{40}Ar/^{39}Ar$ age from *Watts et al.* [1988] (gray font).

10.1029/2011GC003804

with respect to the inlet time of the gas sample into the mass spectrometer. All ages were calculated using the corrected *Steiger and Jäger* [1977] decay constant of 5.530 ± 0.097 × 10^{-10} 1/yr (2σ) as reported by *Min et al.* [2000]. For a detailed description of the analytical facility and the constants used in the age calculations we refer to Table 2 in the work by *Koppers et al.* [2003a]. Incremental heating plateau ages and isochron ages were calculated as weighted means with $1/\sigma^2$ as weighting factor [*Koppers et al.*, 2003a; *Taylor*, 1997] and as YORK2 least squares fits with correlated errors [*York*, 1968] using the ArArCALC v2.5.1 software from *Koppers* [2002] available from the http://earthref.org/tools/ararcalc.htm website. Plateau ages and isochrons with MSWD values higher than 1 were taken to indicate an increased scatter due to geological uncertainties beyond the precision of the increment ages themselves. In these cases, the reported analytical errors are multiplied by the √MSWD [*Kullerud*, 1991; *York*, 1968]. In this paper, all errors on the $^{40}Ar/^{39}Ar$ ages are reported at the 95% confidence level (2σ), unless otherwise indicated.

3.3. Age Reproducibility

[12] Submarine samples typically are subjected to some (high) degree of alteration. However, the Louisville seamount samples recovered with the AMAT cruise and age dated in this study show relatively minor effects of hydrothermal and seawater alteration, because many are aphyric basalts of low vesicularity, which prevented much post-eruption fluid flow and thus shielded these samples from severe alteration. This resistance to alteration is evident in the very good age reproducibility of the samples analyzed. In two instances we could compare co-magmatic phenocrystic plagioclase to groundmass ages (Table 2). For AMAT 30D-8 this resulted in duplicate ages of 26.3 ± 0.3 Ma (plag) and 26.2 ± 0.2 Ma (gm), similar on the 2σ uncertainty levels, and for AMAT 20D-17 this yielded concordant ages of 39.9 ± 0.6 Ma (plag) and 39.6 ± 0.3 Ma (gm). We also found that in many cases multiple samples from within a single dredge haul or from a particular seamount have excellent reproducibility. Good examples are dredge haul AMAT 10D, which resulted in three reproducible ages of 50.1 ± 0.4, 49.4 ± 0.6 and 50.2 ± 0.5 Ma, or the dredge hauls AMAT 32D and 33D from Rumyantsev (155.9°W) seamount, which gave ages of 21.7 ± 0.3, 21.5 ± 0.2, 21.6 ± 0.2 and 21.3 ± 0.2 Ma (Table 2). In other cases, multiple ages from a single seamount may show an extended age range, likely representing prolonged volcanism on these volcanoes.

4. $^{40}Ar/^{39}Ar$ Results

[13] To achieve the highest possible precision in the $^{40}Ar/^{39}Ar$ age determinations, and to be able to identify samples with any alteration remaining after our intensive acid leaching procedure, a large number of heating steps were carried out for each sample (Figure 2). For groundmass samples we performed incremental heating experiments with 21–44 steps and for the plagioclase mineral separates with 10–12 steps. For the groundmass samples we also increased the number of low temperature heating steps (with laser intensities below 0.05 W) to ensure an effective removal of any remaining alteration and atmospheric contamination. Typically, after 8 to 15 low temperature steps, an adequate amount of these discordant gasses were released, allowing us to discern horizontal age plateaus with reproducible, primary crystallization or eruption ages. Using this approach, between 5 and 22 (on average 11) of the heating steps define the age plateaus that also include from 30% to 90% (on average 56%) of the $^{39}Ar_K$ gas released. Only 9 of the 37 groundmasses yielded age plateaus with less than 50% of the total amount of $^{39}Ar_K$ gas released. Our approach resulted in high precision ages (with nominally 0.6–1.2% 2σ uncertainties, including J-value errors) that are reproducible between separates of the same sample, between samples from the same dredge haul, and in some cases between samples from different dredge hauls on a single seamount (Figure 3).

[14] All Louisville groundmasses analyzed are characterized by relatively high K/Ca ratios (on average 0.24, but ranging up to 0.51), and therefore most of the resulting age plateaus also are characterized by high radiogenic ^{40}Ar contents. This makes carrying out the isochron calculations difficult (or impossible) as the data points show little dispersion and plot (very) close to the radiogenic age intercept on an inverse isochron, for example (Text S1). However, the data from the few groundmass and plagioclase analyses that could be used for isochron calculations show that the $^{40}Ar/^{36}Ar$ intercepts are close to the 295.5 value of atmospheric argon, although these calculations comprised a higher level of uncertainty (Table 2). The relatively high abundance of primary magmatic potassium in these rocks is also evident in the age plateaus as these are characterized by K/Ca values on average 56% and maximally 128% higher than the "bulk" total fusion K/Ca values. More than 90% of the groundmass

samples have age plateau K/Ca values that are higher than their corresponding total fusion values. In addition, 65% of the age plateaus have K/Ca values that are lower than observed during the low temperature steps and 97% are higher than the K/Ca values observed during the high temperature steps (Table 2). These K/Ca systematics are typical for groundmass analyses [*Koppers et al.*, 2004, 2007] [e.g., *Koppers et al.*, 2000] and are indicative of a preferential release of argon from alteration phases at low temperatures, and high-Ca phases (i.e., plagioclase and clinopyroxene) at higher temperatures when the groundmass separates are (partially) being melted using the CO_2 laser. Regardless of these complexities in release behavior, and the lack of meaningful isochrons for groundmass samples, the vast majority of our analyses yielded concordant plateau and total fusion ages. This affords a high confidence in our $^{40}Ar/^{39}Ar$ analyses, showing that the groundmasses did not lose any (or at least not very much) of the radiogenic ^{40}Ar after crystallization, and together with the very good reproducibility discussed above, we therefore conclude that all ages represent eruption ages of these seamount lavas.

5. Discussion

[15] With this study we have added 42 high-precision $^{40}Ar/^{39}Ar$ age determinations to the age distribution of the Louisville seamount trail. Together with nine $^{40}Ar/^{39}Ar$ ages reported by *Koppers et al.* [2004] we now have eruption ages from 25 guyots and seamounts along the Louisville seamount trail, ranging in age from 1.1 to 78.8 Ma (Figure 3). We thus substantially increased the seamount age coverage over the 4,300 km length of this seamount trail. This allows us to map out detailed systematics in the age progression, to compare the Louisville seamount eruption ages with ages of congruent seamounts in the Hawaiian-Emperor trail and with the most recent APM models, and to evaluate the extent of motion between these two hot spots.

5.1. Seamount Ages Versus "Fixed Hot Spot" Plate Motion Models

[16] In Figure 4a, we plot the age-distance relationship for the Louisville seamount trail that shows a systematic age progression (increase) from east to west. In this diagram, great circle distances (in degrees) are measured along the seamount trail, with respect to the 52.4°S and 137.2°W hot spot location [*Wessel et al.*, 2006] and taking into account the "bends" in its morphology. All available $^{40}Ar/^{39}Ar$ ages are then compared to age progressions predicted by recent APM models, assuming that all hot spots remained fixed in the mantle over their life spans. Even though the Hawaiian hot spot has moved significantly over the last 80 Myr [e.g., *Tarduno et al.*, 2003], these comparisons remain insightful and are useful for identifying episodes of different behaviors between multiple hot spot systems. We will discuss some of the shortcomings of fixed hot spot APM models below, and in Section 5.3 we will repeat this exercise by comparing the Louisville ages to a set of alternative APM models that attempt to compensate for the motion of hot spots over geological time.

[17] Here we first compare our results to a representative selection of models from *Wessel et al.* [2006] (W06) and *Wessel and Kroenke* [2008] (WK08A and WK08G), and by two older models from *Koppers et al.* [2001] (K01) and *Duncan and Clague* [1985] (DC85) that disregard the change in orientation only apparent in the Hawaiian Ridge (between Molokai and Loihi) for the last 3 Myr. It is clear that most seamount ages lie above all these APM predictions. In Figure 4b we have plotted the age differences (Δt in Myr) between our measured ages and the predicted ages from the WK08G model. This Δt diagram shows that the measured ages are older than the model ages by on average 2.3 Myr and a maximum of 6 Myr. These deviations seem to gradually decrease eastward toward the young end of the seamount trail. Comparing the same set of seamount ages to the WK08A model (an alternative APM model weighted also to published seamount ages before 2008 and not only morphological constraints) or the older W06 model increases the average Δt to at least 2.6 Myr, with a maximum of ~8 Myr. Comparing to the older K01 and DC85 models increases the age offsets even more, in particular toward the old end of the seamount trail.

[18] Despite the observed offset toward higher ages, the character of the Louisville age distribution is well matched by the WK08G model. At the old end of the seamount trail we added three concordant ages for the 27.6°S Guyot (Volcano 33) at 69.6 ± 0.5, 70.8 ± 0.4 and 70.8 ± 0.4 Ma (Table 2) that are very similar to the 68.9 ± 0.6 Ma age for the SOTW-9-52-1 sample [*Koppers et al.*, 2004] dredged from the same northwestern rift zone (Figure 3). Together with the 76.7–78.8 Ma ages of Osbourn Guyot and the 61.4 ± 0.5 Ma age for the SOTW-9-48-2 sample from Currituck Guyot [*Koppers et al.*, 2004], these measured seamount

10.1029/2011GC003804

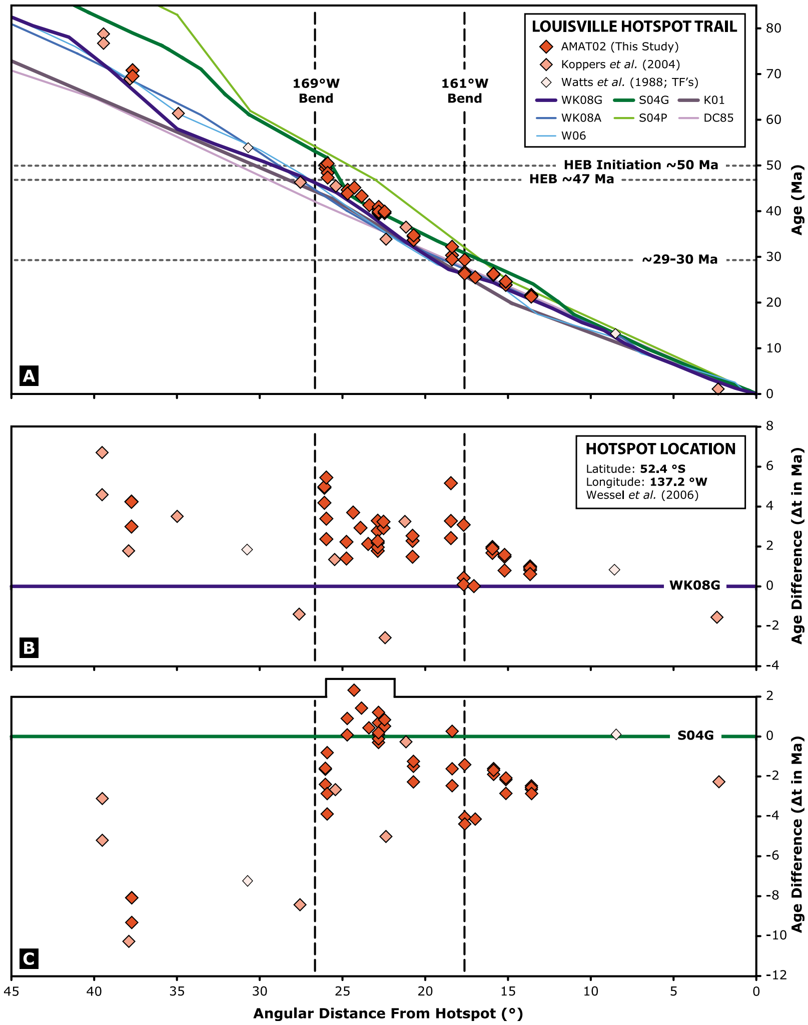

Figure 4. Age versus distance plots for the Louisville seamount trail in comparison to APM models of *Wessel et al.* [2006] (W06), *Wessel and Kroenke* [2008] (WK08A and WK08G), *Koppers et al.* [2001] (K01) and *Duncan and Clague* [1985] (DC85) assuming fixed hot spots, and of *Steinberger et al.* [2004] (S04P and S04G) taking into account moving hot spots. (a) Latitude 52.4°S and longitude 137.2°W are taken as the "zero" age hot spot location in this trail [*Wessel et al.*, 2006]. Distances are calculated as the great circle distance in degrees with respect to this hot spot location and following the shape of the seamount trail. The modeled age progressions assume the same hot spot location at 52.4°S, 137.2°W. (b) Delta age (Δt = measured age − model age) diagram with the age differences calculated between the measured $^{40}Ar/^{39}Ar$ ages and the predicted ages from the WK08G APM model assuming fixed hot spots. The measured ages are up to 6 Myr older than predicted by the WK08G model. (c) Delta age (Δt) diagram with reference to the S04G APM model that takes into account the potential movement of four globally distributed hot spots. The fit between the measured ages and this model is much better, with a maximum (positive) of only 2.3 Myr offset.

ages draw a line parallel (but offset to higher ages) with two WK08G stage poles for Pacific plate motion between 78 and 58 Ma. In a similar way, most of the seamount ages between 50 and 30 Ma more or less track the shape of the WK08G model. Because the WK08G model incorporates a large number of Pacific seamount trails (12 over the last 145 Myr), the plotted (dark blue) line in Figure 4a is a prediction of the "average" Pacific plate motion, assuming all hot spots in the Pacific have remained fixed over the last 80 Myr. Any change in the slope of the WK08G line is either a direct result of a change in the angular velocity of the rotating Pacific plate, a coordinated change in the motion of all Pacific hot spots, or a combination of both. In all three cases, any change, or combination of changes, should be reflected in the locally recorded age progression of the Louisville seamount trail (and any other coeval seamount trail produced on the Pacific plate). If we fit a line through the oldest

Louisville seamount ages, it becomes clear that these seamounts are recording the same "apparent" slow-downs and speed-ups in the Pacific plate motion as predicted by the WK08G model, and by extension, all seamount trails across the Pacific. Apart from assuming fixed or non-fixed hot spots, the detailed age pattern we provide in this paper therefore confirms that the Louisville age progression is non-linear when viewed over its entire ~80 Myr history [*Koppers et al.*, 2004]. The pattern is analogous to the segmented age progression of the Hawaiian-Emperor seamount trail [*Duncan and Keller*, 2004]. This may indicate that congruent changes in rotations and/or speeds for the Pacific plate were recorded by the two longest-lived hot spot trails in the Pacific. Assuming that hot spot motions are unique and therefore different in direction and timing for different hot spots, it must mean that plate motion and plate motion changes remain important in causing the nonlinear character of the Louisville and Hawaiian-Emperor age progressions.

[19] When compared to the "geometrically-optimized" WK08G model of *Wessel and Kroenke* [2008], the measured Louisville seamount ages thus are up to 6 Myr older (Figure 4). However, the fit of the WK08G model seems better for Hawaiian seamounts formed between 0 and 65 Ma (Figure 5a). Analyzing the Δt diagram therefore shows that most of Hawaiian ages are younger than the model ages as indicated by an average offset of only −0.5 Myr (Figure 5b). There is, however, more spread in the Hawaiian data, with a maximum of ~4.2 Myr (ignoring the ~7 Myr older 26.6 Ma age for Northampton Bank) and a minimum of −6.7 Myr (mostly due to younger post-shield ages encountered at the Emperor seamounts of Detroit and Suiko). Although the overall fit of the ages with the WK08G model seems to be good, there are notable exceptions, with seamounts around the 50 Ma Hawaiian-Emperor bend (HEB) being slightly older than the model predictions, the five ages between 30 and 15 Ma showing a considerable amount of (unidentified) scatter, and most of the shield-building ages from the <12 Ma Hawaiian Ridge volcanoes plotting below the WK08G model line. In addition, toward the old end of the Emperors, the Hawaiian seamount ages seem to get systematically younger, which is surprising because the ages included in this compilation (including ~78 Ma Detroit Guyot) are by and large from the shield-building stage and some post-shield lavas (which provides a younger age limit for the tholeiitic shield stage).

[20] For easy comparison, we also plotted the Louisville and Hawaiian seamount ages against the opening angle (ω) of the Pacific plate over time (Figure 6a) as calculated with reference to the WK08G plate rotations. This allows us to plot both age data sets within a single diagram, and if these hot spots are fixed, they should be indistinguishable from the WK08G model and overlie each other. It is clear, however, that neither are the data sets identical nor in agreement with the WK08G model. This is most clearly shown in the Δt diagram (Figure 6b), with most of the Louisville data displaying positive Δt values and the Hawaiian data displaying more negative Δt values. Even though ages in the seamount trails younger than 20 Ma fall close to the WK08G line (during a time interval in which many sub-parallel seamount trails were active in the Pacific basin), discrepancies increase with age and are most evident prior to 35 Ma for seamounts having a larger than 30° opening angle.

[21] It is no surprise, however, that the age systematics observed for both Louisville and Hawaii do not agree with each other or with the fixed hot spot APM models for three reasons. First, it is important to realize that the average plate motions captured in these models harbor variations derived from differences in the individual seamount trail morphologies and age progressions. These differences are real and exemplified in data for Pacific seamounts younger than 15 Ma that show a very large variation in age progressions, ranging from 7.6 to 12.8 cm/yr among at least seven Pacific seamount trails [*Koppers et al.*, 2011, Figure 6]. It is still unclear what causes such large differences in the age progressions between multiple hot spot systems, but different styles in the volcanic construction of seamounts and a possible control by lithospheric structure may play an important role. Second, the fixed hot spot APM models (W06, WK08G, WK08A, K01, DC85) all ignore the fact that the Hawaiian hot spot incurred a large motion itself between 80 and 50 Ma [*Kono*, 1980; *Tarduno et al.*, 2009, 2003]. For that reason these APM models don't work well prior to 50 Ma, as is revealed by the failure of the Emperor seamounts to "backtrack" to the present-day location of the Hawaiian hot spot close to the Big Island [*Doubrovine and Tarduno*, 2008b]. Even though Hawaii may be the only hot spot incurring such a significant amount of hot spot motion, the APM models effectively should be corrected for these motions (see Section 5.3 for such a comparison). The fact that we see the largest offsets in seamount ages between Louisville, Hawaii and the WK08G model between 80 and 50 Ma shows us that various

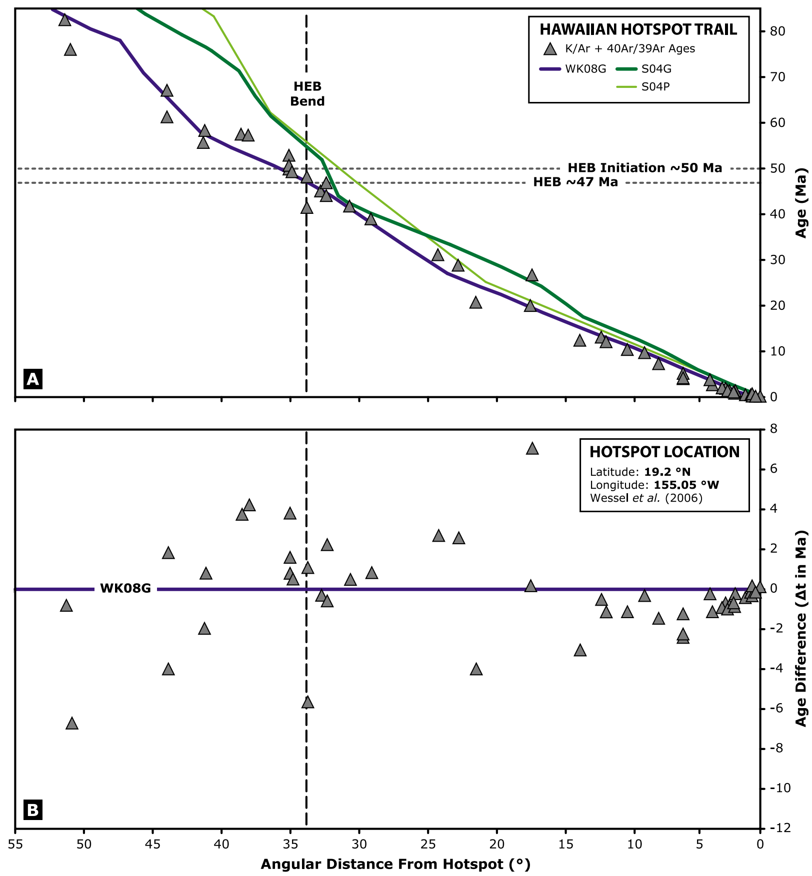

Figure 5. Age versus distance plots for the Hawaiian seamount trail in comparison to recent APM models of *Wessel and Kroenke* [2008] (WK08A and WK08G) assuming fixed hot spots and of *Steinberger et al.* [2004] (S04P and S04G) taking into account moving hot spots. (a) Latitude 19.2°N and longitude 155.05°W are taken as the "zero" age volcano in this hot spot trail [*Wessel et al.*, 2006]. Distances are calculated as the great circle distance in degrees with respect to this active volcano and following the shape of the seamount trail. (b) Delta age (Δt) diagram with the age differences calculated between the measured $^{40}Ar/^{39}Ar$ ages and the predicted ages from the WK08G APM model. The measured ages show increased scatter around the ages predicted from the WK08G model, with ages from 0 to 15 Ma systematically younger while those around the HEB are predominantly too old. All the Hawaiian ages have been recalibrated to FCT-3 biotite (28.03 ± 0.18 Ma, 1σ) as calibrated by *Renne et al.* [1998] using the ArArCALIBRATIONS software from A. A. P. Koppers (see http://earthref.org/tools/ararcalc.htm to download this Microsoft Excel tool).

amounts of hot spot motions need to be considered in this time period and between these two hot spots. Third, the magmatic progression of volcanism on the Louisville seamount trail is enigmatic, with no tholeiitic lavas being recovered in over 70 dredge hauls [e.g., *Hawkins et al.*, 1987; *Vanderkluysen et al.*, 2007] and six IODP drill sites [*Expedition 330 Scientists*, 2011]. This may signify that shield-building stage lavas have not been recovered yet, although that possibility seems remote considering the large sample suite now available for most of the Louisville seamount trail. If all Louisville samples dated in this study represent late-stage lava flows, the $^{40}Ar/^{39}Ar$ ages would be minimum estimates for the age of shield-building in individual Louisville volcanoes, which would make the observed age offsets of 6 Myr (see Figures 4 and 6) minimum estimates as well.

[22] Comparing our new Louisville ages against "fixed" hot spot APM models thus is complicated, but these comparisons allow us to ask a couple important questions: What causes the "apparent" slow-downs and speed-ups in the age progressions of the Louisville and Hawaiian seamount trails? Does the Louisville hot spot still exist as a volcano-producing feature, and should its location at 52.4°S and 137.2°W as used in the WK08G model be reconsidered? Does inter–hot spot motion explain the observed maximum ~6 Myr offset between the Louisville ages and the WK08G model? Does Louisville exhibit an equivalent bend to the familiar

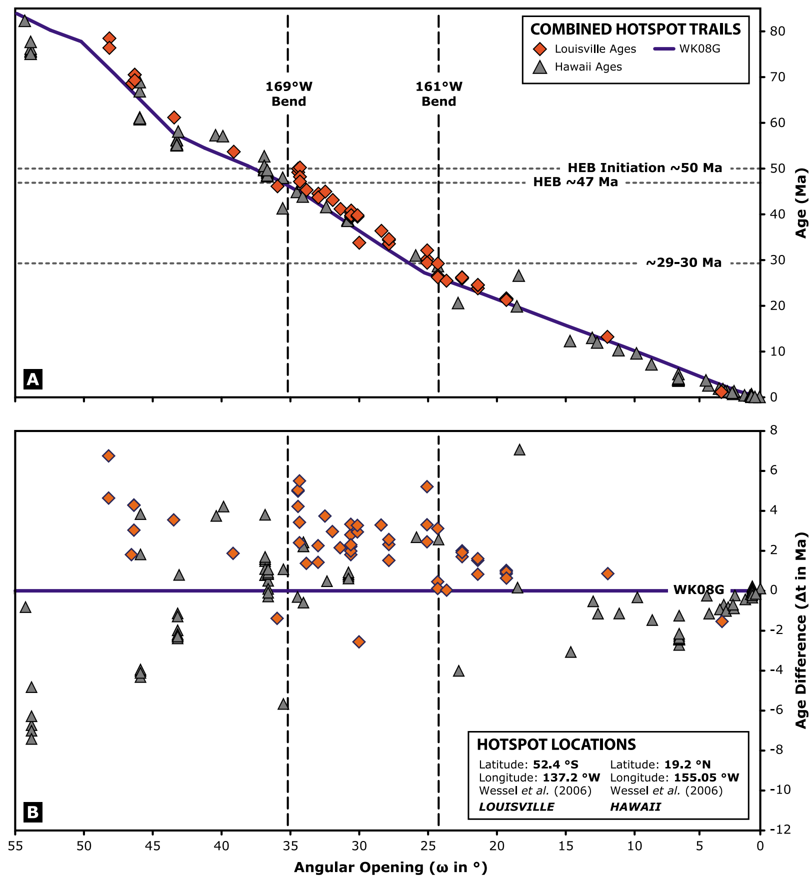

Figure 6. Age versus Pacific plate opening angle for the Louisville and Hawaiian seamount trails in comparison to a recent APM model of *Wessel and Kroenke* [2008] (WK08G). (a) Opening angles are retrieved by interpolating the measured great circle distance between a seamount and either the Louisville (52.4°S, 137.2°W) or Hawaiian (19.2°N, 155.05°W) hot spot to the predicted great circle distances from the *Wessel and Kroenke* [2008] (WK08G) stage pole model. Because the tie-points in the WK08G model between 58 Ma and the present are spaced only 1.3 to 6.4 Myr apart, linear extrapolations are sufficiently accurate when approximating the WK08G opening angles. (b) Delta age (Δt) diagram with the age differences calculated between the measured $^{40}Ar/^{39}Ar$ ages and the predicted ages from the WK08G APM model. The largest differences between the Louisville and Hawaiian age progressions are evident around 70 Ma and after the HEB at 50 Ma.

"elbow" in the Hawaiian-Emperor seamount trail? What are the implications for pre-55 Ma hot spot motions? We address these questions below.

5.2. Continued Existence and Present-Day Location of the Louisville Hot Spot

[23] Satellite altimetry provides little evidence of large (more than 2 km high) volcanoes that might represent the Louisville seamount trail east of 146°W (Figure 7), where there is an unsampled seamount with an estimated age of ~8.5 Ma [*Lonsdale*, 1988]. However, 560 km to the southeast, *Lonsdale* [1988] identified a large, isolated, negatively magnetized volcano, surrounded by a shallow swell. This 139.1°W seamount has an uneroded summit at a depth of 540 m and a single basaltic lava sampled from this summit has the characteristic Louisville geochemical and isotopic signature [*Cheng et al.*, 1987; *Hawkins et al.*, 1987]. Assuming it was a product of the Louisville hot spot, *Lonsdale* [1988] estimated its age as 1.1 Ma, as later confirmed by the 1.11 ± 0.04 Ma $^{40}Ar/^{39}Ar$ age of *Koppers et al.* [2004]. The 139.1°W seamount represents the most convincing evidence that eruptions from the Louisville hot spot continued into the Pleistocene. Whether a belt of small Louisville volcanoes extends across the 560 km "gap" between the 146°W and 139.1°W edifices cannot be determined from existing (paltry) multibeam coverage and (nonexistent) sampling, yet a field of very small seamounts is found along a single narrow multibeam swath (Figure 7a). Nor is there compelling evidence for a younger continuation of the Louisville seamount trail beyond 139.1°W, although a 750 m-high

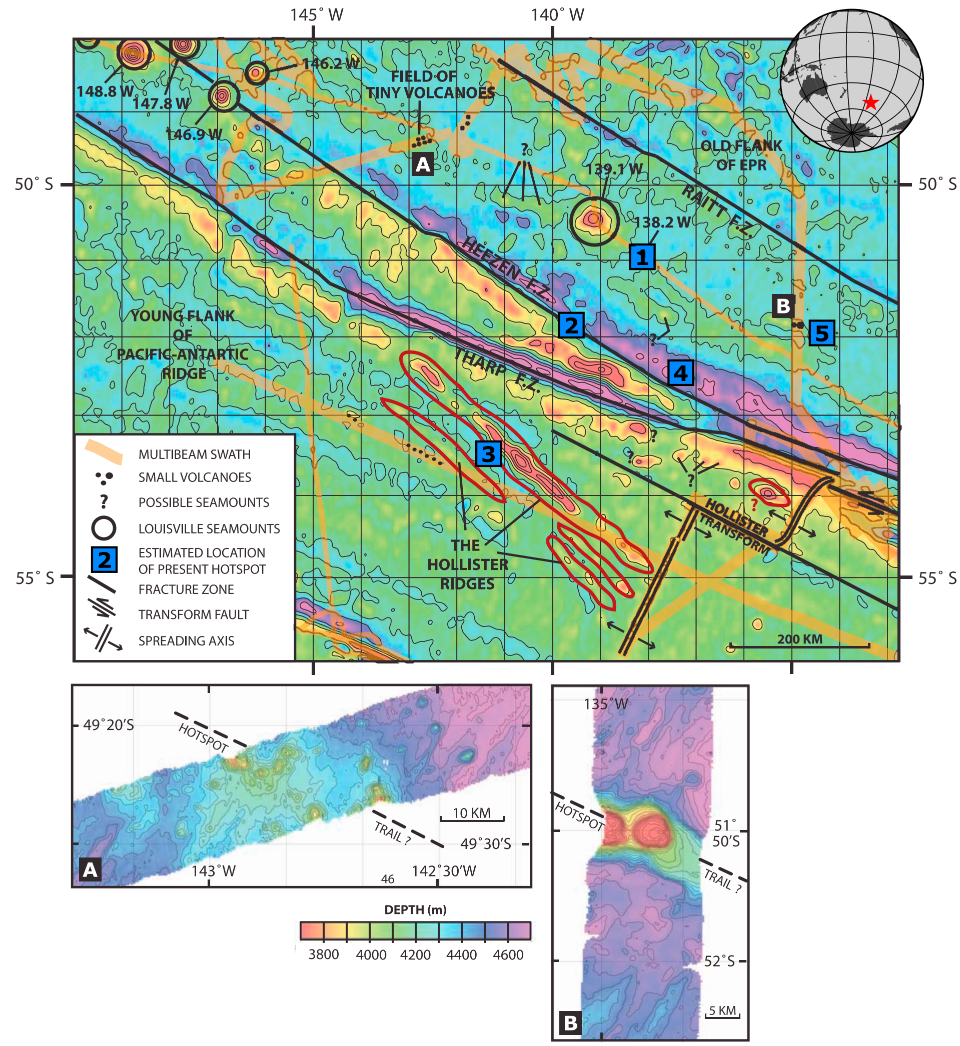

Figure 7. Map of the young end of the Louisville seamount trail where it intersects the Heezen-Tharp fracture zone area. The base map used is the altimetry-derived free-air gravity from *Smith and Sandwell* [1997] with red colors showing gravity highs and purple colors showing gravity lows. The multibeam bathymetry coverage from several Scripps Institution of Oceanography expeditions is shown by orange swath lines. Within these multibeam swaths small volcanoes (which may be related to the Louisville seamount trail) are indicated by black dots, and for two cases (a and b) the volcanoes are shown in detail in the insets. Oblique volcanic ridges on the young west flank of the Pacific-Antarctic Ridge (PAR) labeled the Hollister Ridges [*Small*, 1995] and similar ridges in between the Heezen and Tharp fracture zones, and in between the Hollister transform and the Tharp fracture zone, may have similar non-hot spot origins related to seafloor spreading and the formation of these fault systems [*Lonsdale*, 1986]. On this map we have also plotted the alternative estimates for the present-day location of the Louisville hot spot: [1] 50.9°S, 138.1°W [*Géli et al.*, 1998; *Lonsdale*, 1988]; [2] 51.8°S, 139.5°W [*Watts et al.*, 1988], [3] 53.3°S, 141.2°W ([*Wessel et al.*, 1996] the first "hotspotting estimate"); [4] 52.4°S, 137.2°W ([*Wessel and Kroenke*, 2008] from model WK08G); [5] The new proposed hot spot location at 52.0°S, 134.5°W (this paper) based on best fit to all Louisville seamount ages, with linear extrapolation of the trail beyond 139.1°W seamount. Insets are larger-scale multibeam bathymetry swaths, with 50 m isobaths and the same depth color scale. Figure 7a (inset): A cluster (or band?) of tiny volcanoes interrupting abyssal hill relief midway between the Louisville seamounts at 146.2°W and 139.2°W. Figure 7b (inset): Partial coverage of a chain of 1 km-high unsampled volcanoes near our estimated "best-fit" hot spot location [5].

cratered and unsampled volcano discovered 90 km to the south at 138.2°W might be a candidate for the present-day "zero-age" location of the Louisville hot spot (Location 1 in Figure 7) [*Lonsdale*, 1988].

[24] Geochemical evidence for the continued existence and more recent activity of the Louisville hot spot comes from farther south. Lavas from the Hollister Ridges, a set of oblique fissure-fed ridges

on the young flank of the Pacific-Antarctic Ridge (PAR; Figure 7), and lavas from the PAR itself, have chemical and isotopic compositions that (in particular for Pb isotopes) can be explained by the admixture of a small component of "Louisville" melt to the near-axis asthenosphere [*Castillo et al.*, 1998; *Vlastélic et al.*, 1998]. In this model, the Louisville hot spot mantle may have been channeled to the nearest site of upwelling beneath the PAR, where it contributed to ridge-building eruptions once it passed underneath thinner and younger lithosphere on the western PAR flank [*Castillo et al.*, 1998; *Small*, 1995; *Vlastélic and Dosso*, 2005]. In an initial exposition of their "hotspotting" technique for predicting present-day hot spot locations, *Wessel and Kroenke* [1997] predicted Hollister Ridge as the recent location of the Louisville hot spot (Location 3 in Figure 7). However, we agree with *Vlastélic and Dosso* [2005] that this is mostly precluded by the geochemical evidence, and with *Géli et al.* [1998] and *Koppers et al.* [2001] that the assumption of an abrupt ~3 Ma clockwise change in absolute plate motion, causing an abrupt southward bend in the youngest parts of both the Hawaiian and Louisville hot spot trails, is unrealistic. The hot spotting prediction for the present-day location of the Louisville hot spot used in the more recent WK08G model [*Wessel and Kroenke*, 2008] is much closer to the 139.2°W seamount (Location 4 in Figure 7).

[25] We might argue that the systematic offset to higher ages as shown in Figure 4 could be explained by a mislocation of the present-day location of the Louisville hot spot in the WK08G model. If that location is in fact near the small 138.2°W volcano [*Lonsdale*, 1988], the misfit between the radiometric and WK08G-predicted ages increases to an average Δt of 5.0 Myr. If the WK08G model is to be used for predicting the Louisville seamount ages, it seems that its starting point, the hypothetical present-day site of the hot spot, should be positioned farther east than either *Wessel and Kroenke*'s [2008] hot spotting estimate or the estimate derived from geologic mapping by *Lonsdale* [1988]. We therefore carried out a grid search for a more eastern Louisville hot spot location that would lower the average Δt to a minimum or zero. The "best-fit" solution places the hypothetical Louisville hot spot at 52.0°S and 134.5°W (Location 5 in Figure 7) and brings down the average Δt to 0.0 Myr with a maximum offset of 3.7 Myr (Figure 8). This new hot spot location lies just east of a couple of (unsampled) small volcanoes discovered in another narrow multibeam crossing, which provides some indirect volcanic evidence for this present-day hot spot location (Figure 7b).

5.3. Seamount Ages Versus "Moving Hot Spot" Plate Motion Models

[26] With the southward motion of the Hawaiian hot spot demonstrated from the Emperor Seamounts [*Tarduno et al.*, 2009, 2003] and with predictions from mantle flow modeling by Steinberger and coworkers [*Steinberger and O'Connell*, 1998, 2000], it is now important to take into account the potential motion of hot spots while deriving models for absolute plate motions. *Steinberger et al.* [2004] developed two such models that have been used successfully in later studies; for example, to fit an earlier data set of Louisville seamount ages [*Koppers et al.*, 2004] and to derive a consistent global set of plate motion models [*Torsvik et al.*, 2008]. These models were derived by combining three data sets, namely plate motions with respect to the hot spots, predicted plume motions from mantle flow modeling, and a global set of relative plate motions [e.g., *Steinberger*, 2000]. To some extent this is a circular approach as *Steinberger et al.* [2004] combines density heterogeneities (inferred from tomographic S-wave models) with an APM model to calculate the mantle flow. Vertical plumes are then inserted at depth and get advected into the overall mantle flow regime. This provides hot spot motion trajectories that in turn are used to incrementally correct the initial APM model used. Despite this complexity, their incremental approach provides two useful models for our comparisons: in one they accounted for only the motion of the Hawaii hot spot in the Pacific (S04P) and in another he considered the motion of the Hawaii, Louisville, Reunion and Walvis hot spots globally (S04G). As can be seen in Figure 4a, the fit of these two models is better when compared to the measured Louisville seamount ages. In particular, the global S04G model (dark green line) better describes the oldest ages between 20 and 50 Ma, as is reflected in the Δt diagram of Figure 4c. Because the plotted Louisville seamount ages were *not* corrected for hot spot motion, but the S04G model was by design, it is an important observation that the new Louisville age data fit the S04G model well. This must imply that the Louisville plume did not move significantly over the last 50 Myr. This observation reflects the predictions from mantle flow models that show little plume motion for Louisville over the same period [*Koppers et al.*, 2004; *Steinberger and Antretter*, 2006; *Steinberger et al.*, 2004]. It also reflects the

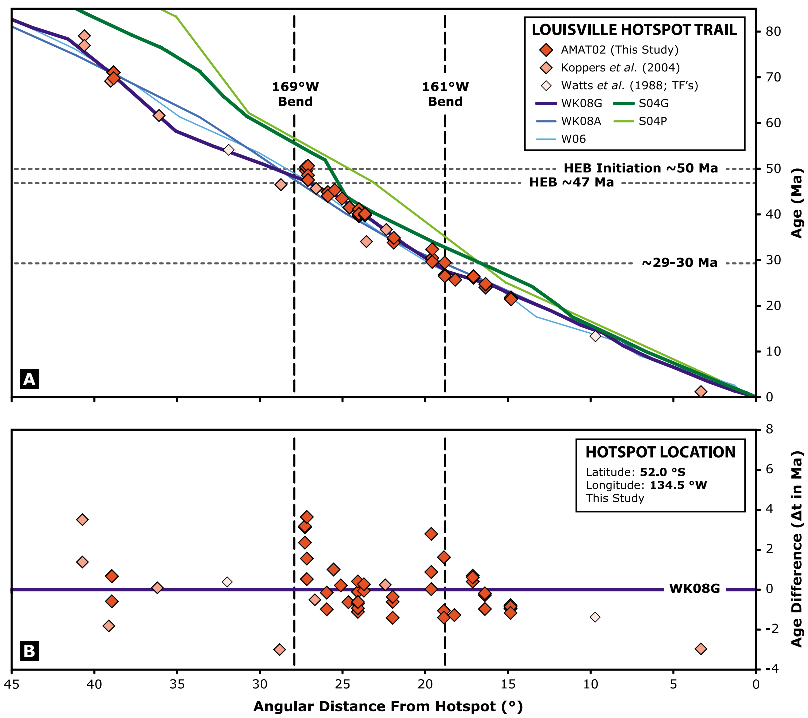

Figure 8. Age versus distance plots for the Louisville seamount trail in comparison to recent APM models of *Wessel and Kroenke* [2008] (WK08A and WK08G) and assuming a new location for the Louisville hot spot. (a) Latitude 52.0°S and longitude 134.5°W are taken as the "zero" age volcano in this hot spot trail (Figure 7). Distances are calculated as the great circle distance in degrees with respect to this active volcano and following the shape of the seamount trail. Clearly an improved fit is visible for the measured ages compared to the WK08G model across the entire seamount trail. However, moving the present-day hot spot more toward the east has significantly degraded the fit to the S04G model of *Steinberger et al.* [2004]. (b) Delta age (Δt) diagram with the age differences calculated between the measured $^{40}Ar/^{39}Ar$ ages and the predicted ages from the WK08G APM model. Because the location of the Louisville hot spot was optimized, the measured ages show less scatter with respect to the WK08G model with an average Δt significantly decreased to zero, however, there is still a maximum offset of ~3.7 Myr.

consistent inter–hot spot distances observed between Hawaiian and Louisville seamounts of similar age [*Wessel and Kroenke*, 2009] that are indicative of little inter–hot spot motion. Together with the lack of any detected Hawaiian plume motion after 50 Ma [e.g., *Sager et al.*, 2005], these observations strongly limit the likelihood of any significant motion of the Louisville hot spot since 50 Ma. On the other hand, in the period prior to 50 Ma the fit of seamount ages to the S04G model is not good, with Δt offsets up to 10 Myr younger (Figure 4c), providing clues about a possible stronger component of Louisville and/or Hawaiian hot spot motion not resolved in the S04G model.

5.4. Determining the Hawaiian-Emperor Bend Equivalent Age

[27] Two slight bends have been recognized in the morphology of the Louisville seamount trail (Figure 1) [*Lonsdale*, 1988]. The "younger" bend is located at 43.95°S and 160.6°W, 1,987 km from the Louisville hot spot, and does not have an obvious equivalent in the Hawaiian seamount trail (or any other trail in the Pacific). The "older" bend is typically considered an equivalent to the HEB and is located at 37.6°S and 169.1°W, 2,985 km from the hot spot (Figures 3 and 4). The 169°W bend was first recognized by *Hayes and Ewing* [1971] and *Epp* [1978] originally placed it around 39.2°S and 167.5°W at a break in the trend resulting from his APM model of the Pacific plate. Overall the 169°W bend causes a gentler angle (170°) in the Louisville seamount trail than the HEB (145°). This makes the determination of the most acute part of this bend more difficult and only possible by interpolation over extended distances along the seamount trail. The 169°W bend area also is more complicated because seamounts located just to the northwest seem to step off the trail axis (and slightly toward the northeast) just prior to the 169°W bend (Figure 3).

[28] With this study we add six new ages east of the 169°W bend for two small neighboring seamounts (Figures 3 and 4a) that at best provide age constraints for the final part of the "bending" in the Louisville seamount trail. These new ages include three concordant ages of AMAT 10D (50.1 ± 0.4, 49.4 ± 0.6 and 50.2 ± 0.5 Ma) and three ages of AMAT 7D (50.9 ± 0.5, 48.4 ± 0.3 and 47.4 ± 0.5 Ma). The maximum ages of 50.2 and 50.9 Ma for these two seamounts are remarkably close to the 50 Ma "initiation age" of the HEB [*Sharp and Clague*, 2006] that in contrast is defining the beginning part of the bending in the Hawaiian-Emperor seamount trail. The ~50–51 Ma age in the Louisville seamount trail thus reflects an entirely different stage in the bending process, the end instead of the beginning, when compared to the HEB initiation age determined by *Sharp and Clague* [2006]. We conclude it is unlikely that the 169°W bend and the HEB were formed contemporaneously, as our new ages are at minimum 3 Myr older than the most acute bend in the Hawaiian-Emperor seamount trail, estimated around 47 Ma (Figure 4a). New ages to the west of the 169°W bend are required if we are to estimate the best possible HEB-equivalent age for the Louisville hot spot and the most accurate difference in the timing between these two bends.

[29] It is important to note that sometimes significant age ranges are observed within single volcanoes and between adjacent volcanoes in parts of the Louisville seamount trail, also near the 169°W bend. As can be seen in Figure 3, samples dredged from the two small guyots east of the 169°W bend are as much as 6 Myr older than rocks of similar (alkalic basalt) chemistry from the adjacent larger guyot, with ages ranging from 47.4 to 50.9 Ma on the smaller seamounts versus 45.5 ± 0.8 Ma on the larger one. This implies long eruptive histories, in particular for this one larger Louisville volcano. Dating superficial (dredged) samples of lavas from volcanoes therefore may lead to significant underestimates for the time that hot spot volcanism began at these sites. Current evidence suggests that the main shield-building stage of (large) Louisville volcanoes is longer than at their Hawaiian-Emperor (tholeiitic) counterparts, even without having determined the ages for some obviously post-erosional lavas in the Louisville seamount trail, which occur in parasitic cones that rise hundreds of meters above some of the guyot summit plains [*Lonsdale*, 1988]. Taking this into account, age discrepancies between congruent volcanoes in the Louisville and Hawaiian-Emperor seamount trails – and in particular the 169°W and HEB bends – would be even greater, if indeed older shield-building lavas exist for these Louisville seamounts.

5.5. Eruption Histories

[30] The Louisville and Hawaiian seamount trails have recorded dissimilar eruption histories (Figure 9) differing by an order of magnitude in their overall output volumes of 130×10^3 and $1,080 \times 10^3$ km^3, respectively. The seamount volumes used in this discussion are not corrected for plate flexure, mass wasting or erosion (i.e., many are guyots) and simply are taken as the volumes of the remaining structures above the surrounding seafloor. The bathymetric data used are from the Seamount Catalog (http://earthref.org) and based on the AMAT02 Expedition and other available multibeam surveys. From these volume calculations it is evident that in some periods their relative magma production rates were similar (Intervals 1 and 3 in Figure 9) and in others when these rates were quite different. A good example is the marked change in magmatic output surrounding the HEB around ~50 Ma (Interval 2 in Figure 9), during which period magma production by the Hawaiian hot spot decreased sharply while Louisville maintained its rate. In contrast, the already lower magma production by the Louisville hot spot started to diminish sharply around 20 Ma (Interval 4 in Figure 9) and seems to have come to a complete halt today, while the relative magma production rates increased significantly for the Hawaiian hot spot since 5 Ma (Interval 6 in Figure 9). Another interesting difference is revealed by the number of seamounts formed over time by these two hot spot systems, whereby the Louisville produced considerably lower numbers than Hawaii, in particular for the last 30 Myr, when only a few Louisville seamounts formed. The Hawaiian hot spot has always produced many more seamounts in each geological interval, except for a short ~15 Myr period after the HEB formed.

[31] There thus seems little connection between magma production rates and numbers of seamounts formed in both the Louisville and Hawaiian seamount trails. Seamount formation rather seems to be controlled by the structural state of the ocean lithosphere onto which the seamounts were emplaced [e.g., *Lonsdale*, 1988; *Vogt*, 1974] and by an overall order-of-magnitude difference in plume flux between Louisville and Hawaii. For example, the slowdown in production rate and decrease in seamount numbers for Hawaii following the HEB occurred when the hot spot passed a

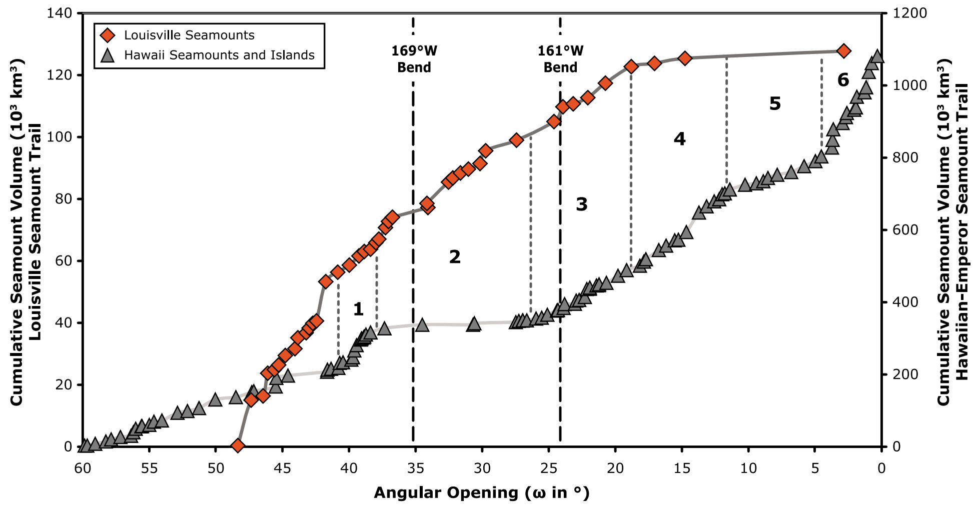

Figure 9. Cumulative volume for the Louisville (left scale) and Hawaiian (right scale) seamount trails. The total volume of Hawaii is an order of magnitude higher than for Louisville. There is no direct link in the (relative) increases or decreases in eruption rate between both seamount trails. Specific more dramatic changes in eruptive volume in either seamount trail are indicated by dashed vertical lines and indicated by numbers 1 through 6 (see text for discussion). Volumes from the Seamount Catalog at http://earthref.org [*Koppers et al.*, 2010a].

major transform fault boundary in the underlying Pacific plate. Because of the large age difference in the ocean crust there also is an inherent increase in plate thickness across this boundary, prohibiting or at least diminishing magma through-put [e.g., *White*, 1993]. In the case of Louisville, the diminishing effects of a lower magma production are seen only at the younger end, east of the 161°W bend, where the Louisville upwelling arguably was captured or diverted by a secondary flow toward the PAR spreading center. Higher magma production rates are associated with the older portion of the Louisville seamount trail west of the 169°W bend, but interestingly this coincides with relatively old and thus thicker lithosphere, according to the latest seafloor age model [*Müller et al.*, 2008].

6. Summary

[32] With our new $^{40}Ar/^{39}Ar$ ages we now have eruption ages from 25 guyots and seamounts along the Louisville seamount trail, providing evidence for an age-progressive trend between 1.1 and 78.8 Ma. This detailed age mapping also confirms that the Louisville age progression is largely nonlinear and mimics the segmented age progression of the Hawaiian-Emperor seamount trail. This large data set makes possible a direct comparison between these two age progressions and the WK08G absolute plate motion model of for example *Wessel and Kroenke* [2008]. By assuming fixed hot spots we observe that the measured Louisville ages are systematically older than the WK08G predictions with offsets ranging up to 6 Myr. These systematic age deviations from the WK08G model may provide evidence that the Louisville plume is mobile, suggesting a movement that is not "in tandem" with the Hawaiian plume. Alternatively, the current approximation for the location of the Louisville mantle plume (still) may be incorrect, contributing to the systematic offset to higher seamount ages, and if in the future samples from earlier volcanic (shield-building) stages are recovered, these offsets may in fact increase.

[33] A large amount of the 6 Myr offset in the Louisville seamount ages may be eliminated by placing this hot spot farther to the east, and closer to the Pacific-Antarctic Ridge spreading center. Placing the Louisville hot spot at 52°S and 134.5°W significantly improves the fit of the age data between Louisville and the WK08G model, while preserving the constant inter–hot spot angular distance between congruent Louisville and Hawaiian seamounts for the time period between 50 Ma and the present-day [*Wessel and Kroenke*, 2009]. This reduces the necessity of any significant inter–hot spot motion in that time interval. However, this scenario does not provide a complete explanation, as it leaves some large positive offsets up to 3.7 Myr, in particular prior to 50 Ma, suggesting that these two hot spot systems may have experienced different individual hot spot motions.

[34] However, a better fit was achieved when comparing the observed Louisville seamount ages with the S04G Pacific plate motion model that takes into account the motion of the Hawaiian, Louisville, Reunion and Walvis hot spots [*Steinberger et al.*, 2004]. The average deviations between the observed ages and S04G model ages are reduced to a maximum offset of 2.3 Myr, using the 52.4°S and 137.2°W hot spot location of *Wessel et al.* [2006]. The fit is particularly good for seamounts younger than 50 Ma, a period for which there is little predicted motion for the Louisville hot spot [*Koppers et al.*, 2004; *Steinberger and Antretter*, 2006; *Steinberger et al.*, 2004] and little inter–hot spot motion with Hawaii [*Wessel and Kroenke*, 2009]. In this second scenario, there thus is no need to find an alternate hot spot location, but again there are discrepancies in the Louisville age-distance record prior to 50 Ma. This must mean that there is an extra source of inter–hot spot motion between Louisville and the other Pacific hot spots that remains uncorrected in the S04G model.

[35] Our results thus show that the $^{40}Ar/^{39}Ar$ age data for the Louisville seamount trail are more compatible with APM models that attempt to compensate for hot spot motion. The good fit with the S04G model suggests that since 50 Ma inter–hot spot motions between Louisville and Hawaii were minimal, yet the increasing misfit of the seamount ages in the older part of the Louisville seamount trail seems to point to an increased amount of inter–hot spot motion, an end-member scenario that is currently being tested by IODP Expedition 330 for the time interval between 80 and 50 Ma [*Koppers et al.*, 2010b]. Our results also show that using WK08G or any other fixed hot spot APM model simply may be incorrect, especially prior to 50 Ma, a period for which these models do not correct the large motion experienced by the Hawaiian hot spot.

[36] Finally, the 169°W bend in the Louisville seamount trail appears to not be equivalent in its age to the HEB. The age for the most acute part of the 169°W bend is slightly older than 50 Ma based on interpolation of our new data, which is at least 3 Myr older than the identical acute part of the HEB. This difference in timing would increase if our dated samples do not represent shield-building (but only late-stage) lavas for the Louisville seamount trail. Both bends thus appear to be asynchronous, which would require other processes (e.g., plume motions) in addition to a global plate motion change to explain this ~50 Ma phenomenon. Differences in magma production rates for the Louisville and Hawaiian hot spot systems are unrelated to the formation of these bends, but seem largely controlled by local structures in the ocean crust and the magnitude of the mantle plume flux itself.

Acknowledgments

[37] Financial support is provided by NSF-OCE 0351512. Lauren Colwell was supported by REU support from NSF-IODP and Molly Gowen by the OSU REU program in 2008. We thank Jake Perez and Loyc Vanderkluysen for their unlimited hard work during the AMAT02RR cruise. Christoph Beier, Kaj Hoernle and an anonymous reviewer are thanked for their very useful comments and suggestions. Erica Pitcavage is thanked for carrying out experiments during her OSU REU summer project of 2009. We thank John Huard for technical support in the OSU argon dating laboratory.

References

Ballance, P. F., D. W. Scholl, T. L. Vallier, A. J. Stevenson, H. Ryan, and R. H. Herzer (1989), Subduction of a Late Cretaceous seamount of the Louisville Ridge at the Tonga Trench: A model of normal and accelerated tectonic erosion, *Tectonics*, *8*(5), 953–962, doi:10.1029/TC008i005p00953.

Beier, C., L. Vanderkluysen, M. Regelous, J. J. Mahoney, and D. Garbe-Schönberg (2011), Lithospheric control on geochemical composition along the Louisville Seamount Chain, *Geochem. Geophys. Geosyst.*, *12*, Q0AM01, doi:10.1029/2011GC003690.

Cande, S. C., C. A. Raymond, J. Stock, and W. F. Haxby (1995), Geophysics of the Pitman Fracture Zone and Pacific-Antarctic plate motions during the Cenozoic, *Science*, *270*(5238), 947–953, doi:10.1126/science.270.5238.947.

Castillo, P. R., J. H. Natland, Y. Niu, and P. F. Lonsdale (1998), Sr, Nd and Pb isotopic variation along the Pacific-Antarctic risecrest, 53–57°S: Implications for the composition and dynamics of the South Pacific upper mantle, *Earth Planet. Sci. Lett.*, *154*(1–4), 109–125, doi:10.1016/S0012-821X(97)00172-6.

Cheng, Q., K.-H. Park, J. D. MacDougall, A. Zindler, G. W. Lugmair, J. Hawkins, P. Lonsdale, and H. Staudigel (1987), Isotopic evidence for a hotspot origin of the Louisville Seamount Chain, in *Seamounts, Islands, and Atolls*, *Geophys. Monogr. Ser.*, vol. 43, edited by B. H. Keating et al., pp. 283–296, AGU, Washington, D. C.

Contreras-Reyes, E., I. Grevemeyer, A. B. Watts, L. Planert, E. R. Flueh, and C. Peirce (2010), Crustal intrusion beneath the Louisville hotspot track, *Earth Planet. Sci. Lett.*, *289*, 323–333, doi:10.1016/j.epsl.2009.11.020.

Courtillot, V., A. Davaille, J. Besse, and J. Stock (2003), Three distinct types of hotspots in the Earth's mantle, *Earth Planet. Sci. Lett.*, *205*(3–4), 295–308, doi:10.1016/S0012-821X(02)01048-8.

Davies, D. R., and J. H. Davies (2009), Thermally driven mantle plumes reconcile multiple hot-spot observations, *Earth Planet. Sci. Lett.*, *278*(1–2), 50–54, doi:10.1016/j.epsl.2008.11.027.

Doubrovine, P. V., and J. A. Tarduno (2008a), Linking the Late Cretaceous to Paleogene Pacific plate and the Atlantic bordering continents using plate circuits and paleomagnetic data, *J. Geophys. Res.*, *113*, B07104, doi:10.1029/2008JB005584.

Doubrovine, P. V., and J. A. Tarduno (2008b), A revised kinematic model for the relative motion between Pacific oceanic plates and North America since the Late Cretaceous, *J. Geophys. Res.*, *113*, B12101, doi:10.1029/2008JB005585.

Downey, N. J., J. M. Stock, R. W. Clayton, and S. C. Cande (2007), History of the Cretaceous Osbourn spreading center, *J. Geophys. Res.*, *112*, B04102, doi:10.1029/2006JB004550.

Duncan, R. A., and D. A. Clague (1985), Pacific plate motion recorded by linear volcanic chains, in *The Ocean Basins and Margins*, vol. 7A, *The Pacific Ocean*, edited by A. E. A. Nairn, F. L. Stehli, and S. Uyeda, pp. 89–121, Plenum, New York.

Duncan, R. A., and R. A. Keller (2004), Radiometric ages for basement rocks from the Emperor Seamounts, ODP Leg 197, *Geochem. Geophys. Geosyst.*, *5*, Q08L03, doi:10.1029/2004GC000704.

Epp, D. (1978), Relationships between plate-plate and plate-mantle motion in Pacific, *Eos Trans. AGU*, *59*(12), 1203.

Expedition 330 Scientists (2011), Louisville Seamount Trail: Implications for geodynamic mantle flow models and the geochemical evolution of primary hotspots, *Integr. Ocean Drill. Program Prelim. Rep.*, *330*, doi:10.2204/iodp.pr.330.2011.

Foulger, G. (2007), The "plate" model for the genesis of melting anomalies, in *Plates, Plumes, and Planetary Processes*, edited by G. Foulger and D. M. Jurdy, *Spec. Pap. Geol. Soc. Am.*, *430*, 1–28, doi:10.1130/2007.2430(01).

Foulger, G. R., and J. H. Natland (2003), Is "hotspot" volcanism a consequence of plate tectonics?, *Science*, *300*(5621), 921–922, doi:10.1126/science.1083376.

Géli, L., D. Aslanian, J. L. Olivet, I. Vlastélic, L. Dosso, H. Guillou, and H. Bougault (1998), Location of Louisville hotspot and origin of Hollister ridge: Geophysical constraints, *Earth Planet. Sci. Lett.*, *164*(1–2), 31–40, doi:10.1016/S0012-821X(98)00217-9.

Hawkins, J. W., P. F. Lonsdale, and R. Batiza (1987), Petrologic evolution of the Louisville seamount chain, in *Seamounts, Islands, and Atolls*, *Geophys. Monogr. Ser.*, vol. 43, edited by B. H. Keating et al., pp. 235–254, AGU, Washington, D. C.

Hayes, D. E., and M. Ewing (1971), The Louisville Ridge—A possible extension of the Eltanin Fracture Zone, in *Antarctic Oceanology I*, *Antarct. Res. Ser.*, vol. 15, edited by J. L. Reid, pp. 223–228, AGU, Washington, D. C.

Kono, M. (1980), Paleomagnetism of DSDP Leg 55 basalts and implications for the tectonics of the Pacific plate, *Initial Rep. Deep Sea Drill. Proj.*, *35*, 737–752, doi:10.2973/dsdp.proc.55.135.1980.

Koppers, A. A. P. (2002), ArArCALC—Software for $^{40}Ar/^{39}Ar$ age calculations, *Comput. Geosci.*, *28*(5), 605–619, doi:10.1016/S0098-3004(01)00095-4.

Koppers, A. A. P., and H. Staudigel (2005), Asynchronous bends in Pacific seamount trails: A case for extensional volcanism?, *Science*, *307*, 904–907, doi:10.1126/science.1107260.

Koppers, A. A. P., and A. B. Watts (2010), Intraplate seamounts as a window into deep earth processes, *Oceanography*, *23*(1), 42–57, doi:10.5670/oceanog.2010.61.

Koppers, A. A. P., H. Staudigel, and J. R. Wijbrans (2000), Dating crystalline groundmass separates of altered Cretaceous seamount basalts by the $^{40}Ar/^{39}Ar$ incremental heating technique, *Chem. Geol.*, *166*(1–2), 139–158, doi:10.1016/S0009-2541(99)00188-6.

Koppers, A. A. P., J. P. Morgan, J. W. Morgan, and H. Staudigel (2001), Testing the fixed hotspot hypothesis using $^{40}Ar/^{39}Ar$ age progressions along seamount trails, *Earth Planet. Sci. Lett.*, *185*(3–4), 237–252, doi:10.1016/S0012-821X(00)00387-3.

Koppers, A. A. P., H. Staudigel, and R. A. Duncan (2003a), High-resolution $^{40}Ar/^{39}Ar$ dating of the oldest oceanic basement basalts in the western Pacific basin, *Geochem. Geophys. Geosyst.*, *4*(11), 8914, doi:10.1029/2003GC000574.

Koppers, A. A. P., H. Staudigel, M. S. Pringle, and J. R. Wijbrans (2003b), Short-lived and discontinuous intraplate volcanism in the South Pacific: Hot spots or extensional volcanism?, *Geochem. Geophys. Geosyst.*, *4*(10), 1089, doi:10.1029/2003GC000533.

Koppers, A. A. P., R. A. Duncan, and B. Steinberger (2004), Implications of a non-linear $^{40}Ar/^{39}Ar$ age progression along the Louisville seamount trail for models of fixed and moving hotspots, *Geochem. Geophys. Geosyst.*, *5*, Q06L02, doi:10.1029/2003GC000671.

Koppers, A. A. P., H. Staudigel, J. Phipps Morgan, and R. A. Duncan (2007), Nonlinear $^{40}Ar/^{39}Ar$ age systematics along the Gilbert Ridge and Tokelau Seamount Trail and the timing of the Hawaii-Emperor Bend, *Geochem. Geophys. Geosyst.*, *8*, Q06L13, doi:10.1029/2006GC001489.

Koppers, A. A. P., H. Staudigel, and R. Minnett (2010a), Seamount catalog: Seamount morphology, maps, and data files, *Oceanography*, *23*(1), 37, doi:10.5670/oceanog.2010.88.

Koppers, A. A. P., T. Yamazaki, and J. Geldmacher (2010b), Louisville Seamount Trail: Implications for geodynamic mantle flow models and the geochemical evolution of primary hotspots, *Integr. Ocean Drill. Program Sci. Prospectus*, *330*, doi:10.2204/iodp.sp.330.2010.

Koppers, A. A. P., J. A. Russell, J. Roberts, M. G. Jackson, J. G. Konter, D. J. Wright, H. Staudigel, and S. R. Hart (2011), Age systematics of two young en echelon Samoan volcanic trails, *Geochem. Geophys. Geosyst.*, *12*, Q07025, doi:10.1029/2010GC003438.

Kullerud, L. (1991), On the calculation of isochrons, *Chem. Geol.*, *87*, 115–124.

Lin, S. C., and P. E. van Keken (2006), Dynamics of thermochemical plumes: 2. Complexity of plume structures and its implications for mapping mantle plumes, *Geochem. Geophys. Geosyst.*, *7*, Q03003, doi:10.1029/2005GC001072.

Lonsdale, P. (1986), Tectonic and magmatic ridges in the eltanin fault system, South Pacific, *Mar. Geophys. Res.*, *8*(3), 203–242, doi:10.1007/BF00305484.

Lonsdale, P. (1988), Geography and history of the Louisville Hotspot Chain in the Southwest Pacific, *J. Geophys. Res.*, *93*(B4), 3078–3104, doi:10.1029/JB093iB04p03078.

Lyons, S. N., D. T. Sandwell, and W. H. F. Smith (2000), Three-dimensional estimation of elastic thickness under the Louisville Ridge, *J. Geophys. Res.*, *105*(B6), 13,239–13,252, doi:10.1029/2000JB900065.

Min, K. W., R. Mundil, P. R. Renne, and K. R. Ludwig (2000), A test for systematic errors in $^{40}Ar/^{39}Ar$ geochronology through comparison with U/Pb analysis of a 1.1-Ga rhyolite, *Geochim. Cosmochim. Acta*, *64*(1), 73–98, doi:10.1016/S0016-7037(99)00204-5.

Morgan, W. J. (1972), Deep mantle convection plumes and plate motions, *Am. Assoc. Pet. Geol. Bull.*, *56*, 42–43.

Müller, R. D., M. Sdrolias, C. Gaina, and W. R. Roest (2008), Age, spreading rates, and spreading asymmetry of the world's ocean crust, *Geochem. Geophys. Geosyst.*, *9*, Q04006, doi:10.1029/2007GC001743.

Raymond, C. A., J. M. Stock, and S. C. Cande (2000), Fast paleogene motion of the pacific hotspots from revised global plate circuit constraints, in *The History and Dynamics of Global Plate Motions*, *Geophys. Monogr. Ser.*, vol. 121, edited by M. A. Richards, R. G. Gordon, and R. D. van der Hilst, pp. 359–375, AGU, Washington, D. C.

Regelous, M., K. D. Collerson, A. Ewart, and J. I. Wendt (1997), Trace element transport rates in subduction zones: Evidence from Th, Sr and Pb isotope data for Tonga-Kermadec arc lavas, *Earth Planet. Sci. Lett.*, *150*(3–4), 291–302, doi:10.1016/S0012-821X(97)00107-6.

Renne, P. R., C. C. Swisher, A. L. Deino, D. B. Karner, T. L. Owens, and D. J. DePaolo (1998), Intercalibration of standards, absolute ages and uncertainties in ^{40}Ar/^{39}Ar dating, *Chem. Geol.*, *145*(1–2), 117–152, doi:10.1016/S0009-2541(97)00159-9.

Sager, W. W., A. J. Lamarche, and C. Kopp (2005), Paleomagnetic modeling of seamounts near the Hawaiian-Emperor bend, *Tectonophysics*, *405*(1–4), 121–140, doi:10.1016/j.tecto.2005.05.018.

Sharp, W. D., and D. A. Clague (2006), 50-Ma initiation of Hawaiian-Emperor bend records major change in Pacific plate motion, *Science*, *313*(5791), 1281–1284, doi:10.1126/science.1128489.

Small, C. (1995), Observations of ridge-hotspot interactions in the Southern Ocean, *J. Geophys. Res.*, *100*, 17,931–17,946.

Smith, W. H. F., and D. T. Sandwell (1997), Global sea floor topography from satellite altimetry and ship depth soundings, *Science*, *277*, 1956–1962, doi:10.1126/science.277.5334.1956.

Steiger, R. H., and E. Jäger (1977), Subcommission on geochronology: Convention on the use of decay constants in geo- and cosmochronology, *Earth Planet. Sci. Lett.*, *36*, 359–362, doi:10.1016/0012-821X(77)90060-7.

Steinberger, B. (2000), Plumes in a convecting mantle: Models and observations for individual hotspots, *J. Geophys. Res.*, *105*(B5), 11,127–11,152, doi:10.1029/1999JB900398.

Steinberger, B., and M. Antretter (2006), Conduit diameter and buoyant rising speed of mantle plumes: Implications for the motion of hot spots and shape of plume conduits, *Geochem. Geophys. Geosyst.*, *7*, Q11018, doi:10.1029/2006GC001409.

Steinberger, B., and A. R. Calderwood (2006), Models of large-scale viscous flow in the Earth's mantle with constraints from mineral physics and surface observations, *Geophys. J. Int.*, *167*(3), 1461–1481, doi:10.1111/j.1365-246X.2006.03131.x.

Steinberger, B., and R. J. O'Connell (1998), Advection of plumes in mantle flow: Implications for hotspot motion, mantle viscosity and plume distribution, *Geophys. J. Int.*, *132*(2), 412–434, doi:10.1046/j.1365-246x.1998.00447.x.

Steinberger, B., and R. J. O'Connell (2000), Effects of mantle flow on hotspot motion, in *The History and Dynamics of Global Plate Motions*, *Geophys. Monogr. Ser.*, vol. 121, edited by M. A. Richards, R. G. Gordon, and R. D. van der Hilst, pp. 377–398, AGU, Washington, D. C.

Steinberger, B., R. Sutherland, and R. J. O'Connell (2004), Prediction of Emperor-Hawaii seamount locations from a revised model of global plate motion and mantle flow, *Nature*, *430*(6996), 167–173, doi:10.1038/nature02660.

Tarduno, J. A., et al. (2003), The Emperor Seamounts: Southward motion of the Hawaiian hotspot plume in earth's mantle, *Science*, *301*(5636), 1064–1069, doi:10.1126/science.1086442.

Tarduno, J., H.-P. Bunge, N. Sleep, and U. Hansen (2009), The bent Hawaiian-Emperor hotspot track: Inheriting the mantle wind, *Science*, *324*(5923), 50–53, doi:10.1126/science.1161256.

Taylor, J. R. (1997), *An Introduction to Error Analysis*, Univ. Sci. Books, Mill Valley, Calif.

Torsvik, T. H., R. D. Müller, R. Van Der Voo, B. Steinberger, and C. Gaina (2008), Global plate motion frames: Toward a unified model, *Rev. Geophys.*, *46*, RG3004, doi:10.1029/2007RG000227.

Turner, S. P., and C. J. Hawkesworth (1997), Constraints on flux rates and mantle dynamics beneath island arcs from Tonga-Kermadec lava geochemistry, *Nature*, *389*, 568–573, doi:10.1038/39257.

Vanderkluysen, L., J. Mahoney, A. A. P. Koppers, and P. F. Lonsdale (2007), Geochemical Evolution of the Louisville Seamount Chain, *Eos Trans. AGU*, *88*(52), Fall Meet. Suppl., Abstract V42B-06.

Vlastélic, I., and L. Dosso (2005), Initiation of a plume-ridge interaction in the South Pacific recorded by high-precision Pb isotopes along Hollister Ridge, *Geochem. Geophys. Geosyst.*, *6*, Q05011, doi:10.1029/2004GC000902.

Vlastélic, I., L. Dosso, H. Guillou, H. Bougault, L. Géli, J. Etoubleau, and J. L. Joron (1998), Geochemistry of the Hollister Ridge: Relation with the Louisville hotspot and the Pacific-Antarctic Ridge, *Earth Planet. Sci. Lett.*, *160*(3–4), 777–793, doi:10.1016/s0012-821x(98)00127-7.

Vogt, P. R. (1974), Volcano spacing, fractures, and thickness of the lithosphere, *Earth Planet. Sci. Lett.*, *21*, 235–252, doi:10.1016/0012-821X(74)90159-9.

Watts, A. B., J. K. Weissel, R. A. Duncan, and R. L. Larson (1988), Origin of the Louisville Ridge and its relationship to the Eltanin Fracture Zone system, *J. Geophys. Res.*, *93*(B4), 3051–3077, doi:10.1029/JB093iB04p03051.

Wessel, P., and L. Kroenke (1997), A geometric technique for relocating hotspots and refining absolute plate motions, *Nature*, *387*(6631), 365–369, doi:10.1038/387365a0.

Wessel, P., and L. W. Kroenke (2008), Pacific absolute plate motion since 145 Ma: An assessment of the fixed hot spot hypothesis, *J. Geophys. Res.*, *113*, B06101, doi:10.1029/2007JB005499.

Wessel, P., and L. W. Kroenke (2009), Observations of geometry and ages constrain relative motion of Hawaii and Louisville plumes, *Earth Planet. Sci. Lett.*, *284*(3–4), 467–472.

Wessel, P., L. W. Kroenke, and D. Bercovici (1996), Pacific plate motion and undulations in geoid and bathymetry, *Earth Planet. Sci. Lett.*, *140*(1–4), 53–66, doi:10.1016/0012-821x(96)00037-4.

Wessel, P., Y. Harada, and L. Kroenke (2006), Toward a self-consistent, high-resolution absolute plate motion model for the Pacific, *Geochem. Geophys. Geosyst.*, *7*, Q03L12, doi:10.1029/2005GC001000.

White, R. S. (1993), Melt production rates in mantle plumes, *Philos. Trans. R. Soc. London A*, *342*(1663), 137–153, doi:10.1098/rsta.1993.0010.

Wilson, J. T. (1963), A possible origin of the Hawaiian Islands, *Can. J. Phys.*, *41*, 863–870, doi:10.1139/p63-094.

York, D. (1968), Least squares fitting of a straight line with correlated errors, *Earth Planet. Sci. Lett.*, *5*, 320–324, doi:10.1016/S0012-821X(68)80059-7.